DYNAMIC RESPONSE OF MOORED FLOATING BREAKWATERS

by

GLEN ALEXANDER FRASER
B.A.Sc., University of British Columbia, 1975

A THESIS SUBMITTED IN PARTIAL FULFILLMENT OF
THE REQUIREMENTS FOR THE DEGREE OF
MASTER OF APPLIED SCIENCE

in

THE FACULTY OF GRADUATE STUDIES
Department of Civil Engineering

We accept this thesis as conforming
to the required standard

THE UNIVERSITY OF BRITISH COLUMBIA
January 1979

In presenting this thesis in partial fulfillment of the requirements for an advanced degree at the University of British Columbia, I agree that the Library shall make it freely available for reference and study. I further agree that permission for extensive copying of this thesis for scholarly purposes may be granted by the Head of my Department or by his representatives. It is understood that copying or publication of this thesis for financial gain shall not be allowed without my written permission.

Department of Civil Engineering

The University of British Columbia
2075 Wesbrook Place
Vancouver, Canada
V6T 1W5

Date March 15, 1979

ABSTRACT

The problem of finding the response of a moored floating breakwater is examined with particular reference to the effect of the moorings on breakwater motions. A computer program has been developed in which hydrodynamic coefficients are calculated using the finite element method. The complete breakwater-mooring system is modelled using the techniques of plane-frame structural analysis. The importance of the second-order drift force in the mooring analysis is noted. Comparison is made between the motions of an unrestrained floating body and those of a body restrained by slack moorings. A simple approximation for high-frequency motions is proposed.

TABLE OF CONTENTS

LIST OF FIGURES

NOMENCLATURE

A = cross-sectional area of mooring line

$[A]$ = matrix of added mass coefficients

a_{jk} = added mass coefficient

B = beam of breakwater

$[B]$ = matrix of damping coefficients or structure damping matrix

$[b]$ = cable element damping matrix

b_{jk} = damping coefficient

C = unstretched length of mooring line

C_D = drag coefficient of mooring line

c = wave celerity

c_g = wave group velocity

D = draught of breakwater

D_c = diameter of mooring line

d = water depth or cable drag

E = elastic modulus of mooring line

F = force or drag force per unit length of mooring line

F_i = exciting force on body

F_{jk} = force in j direction due to unit amplitude motion in k direction

F_c = Coulomb damping force

F_D = drift force

(F) = cable element nodal force vector

f_{jk} = complex form of F_{jk}

g = acceleration due to gravity

H = horizontal force in mooring line

h = wave height or rise in mooring line

h_i, h_r, h_t = incident, reflected, and transmitted wave heights

I_0 = polar mass moment of inertia per unit length of breakwater about z-axis

I_{zz} = moment of inertia of waterplane area per unit length of breakwater about z-axis

$\underline{i}, \underline{j}$ = unit vectors in x and y directions

K_c = Keulegan-Carpenter number

K_r, K_t = reflection and transmission coefficients

$[K]$ = hydrostatic or structure stiffness matrix

$[K_i]$ = finite element matrices

k = wave number ($k = 2\pi/\lambda$)

$[k]$ = cable element stiffness matrix

L = span of mooring line or length of cable element

ℓ = local coordinate on perimiter of finite element

$[M]$ = mass matrix

m = mass per unit length of breakwater or mooring line

m' = virtual mass per unit length of mooring line

$[m]$ = cable element mass matrix

(N) = vector of interpolation functions

$\underline{n}$ = unit outward normal from fluid region

n_1, n_2 = direction cosines of $\underline{n}$

P = rate of energy transfer per unit width of wave

p = pressure

p_i = pressure due to unit amplitude motion in i^{th} mode

Re = Reynold's number

$\underline{r}$ = position vector of point on body surface

S = fluid boundary or spacing of anchors

S_1 = prescribed velocity boundary or body surface

S_2 = radiation boundary

S_3 = free surface

s = transformed finite element coordinate

T = period of oscillation or tension in mooring line

t = time or transformed finite element coordinate

U_m = maximum horizontal fluid velocity

u, v = fluid velocity in x and y directions

v = lateral velocity of cable element

V_n = normal velocity

V = underwater volume per unit length of breakwater

W_D = rate of energy dissipation in moorings

w_c = buoyant weight per unit length of mooring line

X_i = complex exciting forces

x, y, z = Cartesian coordinates

x_f = x-coordinate of centroid of waterplane area

y_b = y-coordinate of centre of buoyancy

y_g = y-coordinate of centre of gravity

Z = length of breakwater associated with one set of moorings

Δ = elongation of mooring line or log decrement

δ = lateral displacement of mooring line

(δ) = vector of cable element nodal displacements

η = surface elevation

θ = angle of mooring line with sea bed

λ = wavelength

ξ_i = complex amplitudes of body motion

ρ = density of fluid

ρ_c = density of mooring line material

Φ = velocity potential

ϕ = complex velocity potential

ϕ_0 = incident wave potential

ϕ_R = scattered wave potential

ϕ_i = forced motion potentials

(ϕ) = vector of nodal values of ϕ

Ω = domain of fluid region

ω = angular frequency of oscillation

ACKNOWLEDGEMENT

The author wishes to thank Drs. M. De St. Q. Isaacson, M. D. Olson, and R. F. Hooley for their advice and assistance in the preparation of this thesis. Financial support was provided by a National Research Council of Canada Postgraduate Scholarship.

CHAPTER 1

INTRODUCTION

1.1 Introduction

Different types of marine activities require different levels of protection from waves. A harbour may adequately protect large ships from ocean waves, yet the waves generated inside the harbour by wind and ship movements may be objectionable to small craft. As a result it is often necessary to provide additional protection around small craft marinas. This protection need not be effective against long wavelength ocean waves as only shorter wavelengths are present inside the harbour.

Rubble mound breakwaters can be used but they can be expensive, particularly if the water is deep. Also, any solid breakwater interferes with the slow circulation of water in the harbour which may cause sedimentation, erosion, and pollution problems. The advantage of a solid breakwater is that it reflects or absorbs essentially all of the incident waves, regardless of wavelength. In contrast, a floating breakwater allows slow circulation of water underneath the body of the breakwater and the cost is nearly independent of water depth. However, a floating breakwater may or may not be effective in reducing the height of waves in the area it is supposed to protect.

The success of floating breakwaters has been mixed,[1] partially due to problems in predicting the forces on the breakwater and moorings and in predicting the effectiveness of the breakwater in reducing wave heights. The purpose of this thesis is to present a method of analysing a prismatic floating breakwater including the effects of slack mooring lines in order to investigate how the moorings affect the motions and efficiency of the breakwater.

1.2 Survey of Analysis Methods

The analysis procedures for floating breakwaters are extensions of the study of ship motions. The usual method of analysis is to solve for fluid velocities according to linear potential theory. Exact solutions are available only for a few special geometries such as vertical barriers (Dean[2], Ursell[3]).

There are several numerical methods for analysing flow around horizontal cylinders of arbitrary cross-section. The earliest numerical method is that of Ursell[4] in which the potential field is represented by a source function and multipoles at the origin of the coordinate system. The method can be used for circular cylinders and shapes that can be obtained from a circle by conformal mapping.

The most common numerical method is the method of integral equations using Green's functions. The Green's functions, first obtained by John[5], give the potential at any point in the fluid resulting from a point source on the body surface. The boundary condition on the body surface can then be developed into a line integral equation which can be solved numerically to obtain the distribution of source strengths along the body contour. The

Green's functions then give the potential for any point in the fluid region.

A more recent numerical method is the use of finite elements in which the fluid surrounding the body is divided into a number of regions or elements. The method is discussed by Newton[6], Bai[7], Chen and Mei[8], and Bettess and Zienkiewicz[9]. The governing differential equation is expressed in variational form as the minimum of some functional. The potential field is defined by the potential at a finite number of nodes on the element boundaries and by interpolating functions within the elements. Minimizing the functional with respect to the nodal values of the potential gives a set of algebraic equations that can be solved to find the potential field. The finite element method produces a much larger set of equations than the integral equation method for the same degree of accuracy. However, the matrix to be solved in the finite element method is symmetric and banded which allows the use of very efficient solution procedures. Extensions of the finite element method are the hybrid element method of Chen and Mei, and the use of infinite elements developed by Bettess and Zienkiewicz. Both methods reduce the size of the finite element region and thus the order of the matrix to be solved.

Other numerical methods include a variational method (Mei and Black[10]), matched expansions (Takano[11]), and finite differences (Nichols and Hirt[12]).

The fundamental difference between the analysis of ship motions and the analysis of floating breakwaters is that the oscillatory mooring forces significantly affect the body motions

in the latter case. Yamamoto and Yoshida[13] have represented the mooring system by linear springs. Adee and Martin[14] also model the moorings by linear springs but suggest that for ordinary slack moorings, the mooring stiffness may be neglected. Remery and van Oortmerssen[15] suggest that the non-linear behavior of the moorings is important. They state that the total load on the mooring is made up of oscillatory wave forces, which in the linear analysis are proportional to the wave height, and steady wind, current, and wave drift forces which are proportional to the square of the wind velocity, current velocity, and wave height respectively. In this thesis, the mooring analysis suggested by Remery and van Oortmerssen will be applied to the problem of finding the motions of a floating breakwater.

1.3 Description of Method

The analysis procedure which is described in detail in Chapters 2 and 3 may be divided into two parts. The first is the hydrodynamic analysis of an unrestrained floating body. This analysis of fluid motion in the region surrounding the body yields the excitation and response characteristics of the body when subject to an incident wave train. These body characteristics are combined with the mooring system characteristics in the second part of the analysis, which is the structural analysis of the combined body-mooring system. The structural analysis yields the motions of the body-mooring system, from which the desired wave amplitudes, pressures, stresses, and body motions may be calculated.

For the hydrodynamic analysis, a region of fluid surrounding the body is isolated. Fluid motions within the region are described according to potential theory by a differential equation and boundary conditions. The differential equation is solved by the finite element method to give the fluid velocity potential in terms of the incident wave and body motion amplitudes. The Bernoulli equation is used to find the resulting pressures on the body. The pressures are then integrated over the body surface to find the exciting forces due to the incident wave and the forces opposing motion of the body. The opposing forces can be resolved into two components, one resisting acceleration and another resisting velocity. The first involves the added mass of the body and the second the damping.

The added mass and damping coefficients and exciting forces found from the finite element analysis are then combined with the true mass of the body and the hydrostatic stiffness to yield three coupled linear equations of motion for the body. Solution of these equations gives the body motion amplitudes and phase angles. The transmitted and reflected wave heights can then be calculated from the body amplitudes and their respective velocity potential fields. Finally, the steady drift force on the body can be calculated using the principle of momentum conservation and retaining the second-order terms in the Bernoulli equation.

For the structural analysis, the response of the system is assumed to be of two parts. The first is a static response to the steady drift force and any steady wind and current forces. Here, non-linear equations for a catenary are used to find the equilibrium position of the body and moorings. The mooring

lines are then modelled as a series of straight bar elements, each with a mass, added mass and damping. The equations of motion for these bar elements are combined with the equations of motion for the unrestrained body and solved to find the amplitudes of body motion. As for the unrestrained body, the transmitted and reflected wave amplitudes and the steady drift force are then calculated. Since the new drift force is in general different from that used to find the equilibrium configuration of the mooring lines, the procedure is repeated until convergence of the drift force is achieved. Finally, the forces in the mooring lines are calculated, completing the analysis.

CHAPTER 2

HYDRODYNAMIC ANALYSIS

2.1 Introduction

The problem of finding the motion of an unrestrained floating body in the presence of surface waves has been dealt with by many authors. Newman[16], Garrison[17], and Wehausen[18], have discribed the general three-dimensional linear boundary-value problem to be solved in order to obtain fluid velocities and hence pressures on the body and the body motions. Adee and Martin[14] and Yamamoto and Yoshida[13] have described the two-dimensional problem with particular reference to floating breakwaters.

In this chapter the formulation of the two-dimensional boundary-value problem for potential flow with a free surface and the procedure for generating the equations of motion of the body will be reviewed. As well, the finite element method of solving the boundary-value problem will be described.

2.2 Potential Flow

The region of fluid that will be analysed is shown in Figure 1. The breakwater is assumed to be infinitely long in the direction parallel to the wave crests so that the fluid flow is two-dimensional. The fluid surrounding the breakwater is assumed to be inviscid and incompressible and the fluid motion irrotational so that potential flow theory applies. The x-axis is at the still water level and is positive in the direction of wave propogation. The y-axis is positive upward through the centre of buoyancy of the body when in its equilibrium position in still water. The velocity potential $\Phi(x,y,t)$ is defined such that $\partial\Phi/\partial x=u$ and $\partial\Phi/\partial y=v$ where t is time and u and v are the fluid velocities in the x and y directions respectively. It is further assumed that the fluid motions are simple harmonic so that the space and time variables may be separated

$$\Phi(x,y,t)=\mathrm{Re}[\phi(x,y)e^{i\omega t}] \qquad 2.1$$

where ω is the angular frequency of motion.

For the above definition of ϕ the requirements of incompressibility and zero-vorticity result in Laplace's equation

$$\frac{\partial^2\phi}{\partial x^2} + \frac{\partial^2\phi}{\partial y^2} = 0 \qquad 2.2$$

as the governing differential equation to be solved in the fluid region.

The boundary conditions must be expressed in terms of the velocity potential. On the prescribed velocity boundary (S_1), the normal velocity of the boundary (V_n) must equal the normal velocity of the fluid at the boundary. This yields the boundary

condition

$$\frac{\partial \phi}{\partial n} = V_n \qquad \text{on } S_1 \qquad 2.3$$

where n is a unit normal outward from the fluid region. For a fixed boundary, the boundary condition is then

$$\frac{\partial \phi}{\partial n} = 0 \qquad 2.4$$

On the free surface, the pressure is zero relative to atmospheric pressure and the normal velocity of the free surface must equal the normal velocity of a particle at the free surface. The Bernoulli equation may be written as

$$p + \frac{1}{2}\rho(u^2 + v^2) + \rho g y + \rho\frac{\partial \Phi}{\partial t} = 0 \qquad 2.5$$

where p is the pressure, ρ is the density of fluid and g the acceleration due to gravity. Putting p=0 in the Bernoulli equation and neglecting the velocity squared terms as second order gives the zero pressure condition

$$g\eta + \frac{\partial \Phi}{\partial t} = 0 \qquad \text{at } y = 0 \qquad 2.6$$

where η is the surface elevation measured from y=0. The velocity squared terms are neglected as they can be shown to be of the same order as the wave steepness squared. The wave steepness is assumed to be small. For the linear analysis the free surface boundary condition is applied at y=0 rather than at the true free surface $y=\eta$. The linearized kinematic boundary condition, assuming small slope of the surface profile is

$$\frac{\partial \phi}{\partial y} = \frac{\partial \eta}{\partial t} \qquad \text{at } y = 0 \qquad 2.7$$

Combining Equations 2.6 and 2.7 and eliminating η gives the free surface boundary condition

$$\frac{\partial \phi}{\partial n} = \frac{\omega^2}{g}\phi \qquad \text{at } y = 0 \qquad 2.8$$

On the radiation boundary, the potential must have the form of a wave travelling outward from the region. The potential for a plane wave travelling in the +x direction is

$$\Phi = \mathrm{Re}\{\frac{igh}{2\omega}\frac{\cosh(k(y+d))}{\cosh(kd)}e^{i\omega t-ikx}\} \qquad 2.9$$

where h is the wave height, k is the wave number $2\pi/\lambda$, λ the wavelength, and d the depth of water. Not all the variables on the right side of Equation 2.9 are independent as the dispersion relation, relating wave number to wave frequency may be applied. The dispersion relation is

$$\omega^2 = gk \tanh(kd) \qquad 2.10$$

In order to satisfy Equation 2.9 on the positive radiation boundary, Φ must be periodic in $(\omega t-kx)$. This is equivalent to requiring

$$\frac{\partial \Phi}{\partial x} = -\frac{k}{\omega}\frac{\partial \Phi}{\partial t} \qquad 2.11$$

Applying Equation 2.1 to Equation 2.11 gives for the positive radiation boundary

$$\frac{\partial \phi}{\partial x} = -\frac{i\omega}{c}\phi \qquad 2.12$$

where c is the wave celerity $(c=\omega/k)$. The same procedure for a wave travelling in the -x direction gives for the negative radiation boundary

$$\frac{\partial \phi}{\partial x} = \frac{i\omega}{c}\phi \qquad 2.13$$

For vertical boundaries, both Equation 2.12 and 2.13 can be replaced by

$$\frac{\partial \phi}{\partial n} = -\frac{i\omega}{c}\phi \qquad 2.14$$

where n is a unit outward normal from the fluid region.

The degrees of freedom assigned to the body are indicated in Figure 1. j=1 is horizontal displacement (sway), j=2 is vertical displacement (heave), and j=3 is rotation about the origin of the coordinate system (roll). The displacement from the equilibrium position at any time is given by $\mathrm{Re}\{\xi_j e^{i\omega t}\}$ where ξ_j is the complex amplitude in the jth mode. It is assumed that all amplitudes are small in comparison to the size of the body.

The velocity potential in the region surrounding the body is assumed to be of the form

$$\phi = \phi_0 + \phi_R + \sum_{j=1}^{3} \xi_j \phi_j \qquad 2.15$$

where ϕ_0 is the incident wave potential, ϕ_R is the potential of the scattered wave from the fixed body, and ϕ_1, ϕ_2, and ϕ_3 are the forced motion potentials due to unit amplitude sway, heave, and roll respectively in calm water. The incident wave potential from Equation 2.9 is

$$\phi_0 = \frac{igh_i}{2\omega} \frac{\cosh(k(y+d))}{\cosh(kd)} e^{-ikx} \qquad 2.16$$

where the subscript i indicates the incident wave. By this definition a wave crest passes x=0 at $\omega t=0$.

The sum of the normal velocities of the incident and scattered waves at the surface of the fixed body must be zero. This results in the boundary condition

$$\frac{\partial \phi_R}{\partial n} = - \frac{\partial \phi_0}{\partial n} \qquad 2.17$$

on the body surface S_1. The scattered wave potential can then be found by solving the boundary-value problem with $-\partial\phi_0/\partial n$ as

the prescribed velocity on the body surface.

The forced motion potentials can be found in a similar manner. Defining $\underline{r} = x\underline{i} + y\underline{j}$ as the position vector of a point on the body surface and $\underline{n} = n_1\underline{i} + n_2\underline{j}$ as a unit normal vector into the body, a unit amplitude displacement in each mode yields the following prescribed velocities for the body surface, assuming small amplitudes of motion

$$\begin{aligned} \text{sway} \quad & V_n = i\omega n_1 \\ \text{heave} \quad & V_n = i\omega n_2 \\ \text{roll} \quad & V_n = i\omega(\underline{r} \times \underline{n}) \end{aligned} \qquad 2.18$$

In the linear analysis, the boundary condition is applied at the equilibrium position of the body surface rather than at the instantaneous position.

2.3 Exciting Forces, Added Mass, and Damping

The potential flow theory of Section 2.2 is based on the assumption of irrotational flow, hence flow separation and the formation of vortices are not included in the theory. An indication of flow separation and thus the applicability of potential theory in finding the forces on the breakwater is the Keulegan-Carpenter number (K_c). The Keulegan-Carpenter number is proportional to the ratio between the amplitude of fluid particle horizontal displacement and a typical dimension of the body

$$K_c = U_m T/B \qquad 2.19$$

where U_m is the maximum particle horizontal velocity, T is the period of oscillation and B is the beam of the breakwater. For the range of frequencies to be studied, K_c will usually be less

than three. In this range it can be assumed that inertia effects predominate over drag effects, therefore wave forces will be calculated from the potential flow solution. While the potential theory cannot strictly be applied to flow past a rectangular body due to the formation of vortices at the corners, Bearman et al[19] have found that the presence of these vortices has little effect on forces on a square-section cylinder with sides parallel to the incident flow at low values of K_c. Their results suggest that potential flow theory can be used to find the forces on a rectangular section floating breakwater.

The Bernoulli equation (Eqn. 2.5) is linearized by neglecting the velocity squared terms as second order. Also, the hydrostatic pressure gy is omitted so as to give the relation between the potential field and the dynamic pressure p as

$$p = -\rho\frac{\partial\Phi}{\partial t}$$

$$\text{or} \qquad p = -\mathrm{Re}\{i\omega\rho\phi e^{i\omega t}\} \qquad 2.20$$

In the linearized solution, the exciting forces on the body are independent of body motion, thus the exciting forces are the integrals over the equilibrium body surface of the pressure due to the incident and scattered waves only. If the exciting force is of the form

$$F_j = \mathrm{Re}\{X_j e^{i\omega t}\} \qquad j=1,2,3 \qquad 2.21$$

then

$$X_i = -i\omega\rho\int_{S_1}(\phi_0+\phi_R)(\underline{r} \times \underline{n})^{n_i} ds \qquad \begin{matrix} i=1,2 \\ i=3 \end{matrix} \qquad 2.22$$

where S_1 is the equilibrium body surface.

The forces resisting motion of the body can be found by

applying the Bernoulli equation to the forced motion potentials. If F_{jk} is the force in the j direction due to a unit amplitude motion in the k direction and p_k is the pressure due to a unit amplitude motion in the k direction, then

$$F_{jk} = \int_{S_1} p_k (\underline{r} \times \underline{n}^j) ds \qquad \begin{matrix} j=1,2 \\ j=3 \end{matrix} \qquad 2.23$$

If

$$F_{jk} = \mathrm{Re}[f_{jk} e^{i\omega t}] \qquad 2.24$$

then the force can be expressed in terms of the forced motion potentials by

$$f_{jk} = \rho\omega \int_{S_1} \mathrm{Im}(\phi_k)(\underline{r} \times \underline{n}^j) ds - i\rho\omega \int_{S_1} \mathrm{Re}(\phi_k)(\underline{r} \times \underline{n}^j) ds \qquad \begin{matrix} j=1,2 \\ j=3 \end{matrix} \qquad 2.25$$

The force can also be expressed in terms of components opposing acceleration and velocity of the body

$$\xi_k f_{jk} = -a_{jk}\ddot{\xi}_k - b_{jk}\dot{\xi}_k \qquad 2.26$$

where a_{jk} is the added mass coefficient and b_{jk} is the damping coefficient. For a unit amplitude displacement

$$f_{jk} = \omega^2 a_{jk} - i\omega b_{jk} \qquad 2.27$$

Comparing Equations 2.25 and 2.27 yields

$$a_{jk} = \frac{\rho}{\omega} \int_{S_1} \mathrm{Im}(\phi_k)(\underline{r} \times \underline{n}^j) ds \qquad \begin{matrix} j=1,2 \\ j=3 \end{matrix} \qquad 2.28$$

$$b_{jk} = \rho \int_{S_1} \mathrm{Re}(\phi_k)(\underline{r} \times \underline{n}^j) ds \qquad \begin{matrix} j=1,2 \\ j=3 \end{matrix} \qquad 2.29$$

An alternate way of calculating the exciting forces is by the use of Haskind's relations[16]. By applying Green's Theorem,

it is possible to eliminate the scattered wave potential from the expression for exciting forces. This yields

$$X_j = -\rho \int_{S_1} (\phi_0 \frac{\partial \phi_j}{\partial n} - \phi_j \frac{\partial \phi_0}{\partial n}) ds \qquad j=1,2,3 \qquad 2.30$$

2.4 Equations of Motion

The total or virtual mass of the body to be used in the equations of motion is the sum of the actual mass of the body and the added mass defined by Equation 2.28. Since the origin of the coordinate system is not necessarily at the centre of gravity of the body, the mass matrix may contain off-diagonal terms. The mass matrix for the body is

$$[M] = \begin{bmatrix} m & 0 & -my_g \\ 0 & m & 0 \\ -my_g & 0 & I_0 \end{bmatrix} \qquad 2.31$$

where m is the mass per unit length of the body, I_0 is the polar mass moment of inertia about the origin per unit length, and $(0,y_g)$ is the coordinate of the centre of gravity.

The hydrostatic stiffness matrix can be determined by giving the body a small displacement in each of the three modes in turn and calculating the forces required to maintain equilibrium. For small displacements the stiffness matrix is

$$[K] = \begin{bmatrix} 0 & 0 & 0 \\ 0 & \rho g B & \rho g B x_f \\ 0 & \rho g B x_f & \rho g V\{\frac{I_{zz}}{V} + y_b - y_g\} \end{bmatrix} \qquad 2.32$$

where x_f is the centroid of waterplane area, ∇ is the underwater volume, I_{zz} is the moment of inertia of the waterplane area about the z-axis, and $(0,y_b)$ is the coordinate of the centre of buoyancy. ∇ and I_{zz} are calculated for a unit length of breakwater.

The mass and stiffness matrices, added mass and damping coefficients, and exciting forces can be assembled into the equations of motion of the body. If [A] is the matrix of added mass coefficients and [B] is the matrix of damping coefficients, then the equations of motion are

$$\{-\omega^2([M] + [A]) + i\omega[B] + [K]\}(\xi) = (X) \qquad 2.33$$

which can be solved for the complex amplitudes ξ_j.

The amplitudes of motion can then be used to find the transmitted and reflected wave heights. The wave height is related to the velocity potential by

$$h = \frac{2\omega}{g}\,\phi(x,0) \qquad 2.34$$

For the transmitted wave,

$$\phi = \phi_0 + \phi_R + \sum_{j=1}^{3} \xi_j\phi_j \qquad 2.35$$

and is evaluated at the positive radiation boundary. For the reflected wave

$$\phi = \phi_R + \sum_{j=1}^{3} \xi_j\phi_j \qquad 2.36$$

and is evaluated at the negative radiation boundary. The transmission coefficient is defined as the transmitted wave height divided by the incident wave height

$$K_t = \frac{h_t}{h_i} \qquad 2.37$$

From conservation of energy, the rate of energy transfer into the fluid region must equal the rate of energy transfer out of the fluid region. Since the energy in a wave is proportional to the square of the wave height, the incident, transmitted, and reflected wave heights are related by

$$h_i^2 = h_r^2 + h_t^2 \qquad 2.38$$

Similarly, the transmission coefficient and the reflection coefficient K_r, defined as the reflected wave height divided by the incident wave height, are related by

$$K_r^2 + K_t^2 = 1 \qquad 2.39$$

2.5 Drift Force

According to the previous linear theory, the unrestrained body will maintain the same mean position and undergo only simple harmonic motion in the presence of surface waves. In fact, the body will tend to drift in the direction of propogation of the waves due to the presence of higher order forces. This drift force is important when calculating the equilibrium configuration of the moorings.

Maruo[20] has calculated the second order drift force for a two-dimensional body in deep water. Longuet-Higgins[21] has extended this theory to include shallow water and the absorption of energy by the body. The drift force is calculated by considering conservation of momentum of the body and surrounding fluid, including second-order terms. The drift force is the force required on the body to conserve momentum of the combined body-fluid system. The drift force can also be

considered as the force required to maintain the body in a constant mean position. While the drift force varies slowly with time, a time average of the force is calculated and the force is assumed to be steady for further calculations. According to Longuet-Higgins, the drift force is related to wave heights by

$$F_D = \frac{\rho g}{16}\left(1 + \frac{2kd}{\sinh(2kd)}\right)(h_i^2 + h_r^2 - h_t^2) \qquad 2.40$$

Equation 2.38 need not apply when calculating the drift force as energy may be dissipated through the breakwater or mooring system. If no energy is dissipated by the breakwater or moorings, Equation 2.40 may be reduced to

$$F_D = \frac{\rho g}{8}\left(1 + \frac{2kd}{\sinh(2kd)}\right)h_r^2 \qquad 2.41$$

2.6 Finite Element Solution

The finite element method has been used extensively for solving problems in structural mechanics. The method can also be used to solve a variety of steady-state and transient field problems, one of which is the flow of an ideal fluid. The application of finite elements to fluid problems is detailed in Zienkiewicz[22], Segerlind[23], and Newton[6], and will only be described briefly here.

The differential equation to be solved is Laplace's equation

$$\frac{\partial^2 \phi}{\partial x^2} + \frac{\partial^2 \phi}{\partial y^2} = 0 \qquad 2.42$$

The boundary conditions can be expressed in the form

$$\frac{\partial \phi}{\partial n} + q + a\phi = 0 \qquad 2.43$$

On the various boundaries, the values of q and a are:

fixed boundary	$q = 0$	$a = 0$
prescribed velocity boundary	$q = -V_n$	$a = 0$
free surface	$q = 0$	$a = -\omega^2/g$
radiation boundary	$q = 0$	$a = i\omega/c$

From the calculus of variations or Galerkin's method[22], the solution to the above differential equation and boundary conditions is the function that minimizes the functional

$$\pi = \int_{\Omega} \frac{1}{2}\left(\left(\frac{\partial\phi}{\partial x}\right)^2 + \left(\frac{\partial\phi}{\partial y}\right)^2\right) dxdy + \int_S \left(q\phi + \frac{1}{2}a\phi^2\right) d\ell \qquad 2.44$$

where Ω is the domain of the fluid and S is the entire boundary of the fluid.

In the finite element method, the domain is divided up into a finite number of regions or elements. Figure 2 shows a typical finite element mesh for a rectangular breakwater. Each element has nodes on the boundary where the value of the variable ϕ is matched to adjacent elements. Within any element the potential ϕ can be expressed as $(N)^T(\phi)_e$ where (N) is a column vector of interpolation functions and $(\phi)_e$ is a column vector of nodal values of ϕ. The particular quadratic isoparametric element used here is described in Appendix A.

For an element, minimizing π with respect to the nodal values of ϕ gives the element equation

$$\frac{\partial\pi}{\partial(\phi)_e} = \int_{\Omega_e} \left(\left(\frac{\partial N}{\partial x}\right)\left(\frac{\partial N}{\partial x}\right)^T + \left(\frac{\partial N}{\partial y}\right)\left(\frac{\partial N}{\partial y}\right)^T\right) dxdy\,(\phi)_e + \int_{S_{1e}} q(N)\,d\ell$$
$$+ \int_{S_{2e}+S_{3e}} a(N)(N)^T d\ell\,(\phi)_e = 0 \qquad 2.45$$

The subscript e denotes integration over one element only. S_1 is the body surface, S_2 is the radiation boundary and S_3 is the free surface. The element equations are assembled using standard finite element techniques to produce the global equations.

Inserting the appropriate values of q and a, the global equations are

$$\{\int_{\Omega} [(\frac{\partial N}{\partial x})(\frac{\partial N}{\partial x})^T + (\frac{\partial N}{\partial y})(\frac{\partial N}{\partial y})^T]dxdy + \int_{S_2} \frac{i\omega}{c}(N)(N)^T d\ell$$

$$- \int_{S_3} \frac{\omega^2}{g}(N)(N)^T d\ell\}(\phi) = \int_{S_1} V_n(N)d\ell \qquad 2.46$$

This can be written as the matrix equation

$$\{-\omega^2[K_3] + i\omega[K_2] + [K_1]\}(\phi) = (P) \qquad 2.47$$

where

$$[K_1] = \int_{\Omega} [(\frac{\partial N}{\partial x})(\frac{\partial N}{\partial x})^T + (\frac{\partial N}{\partial y})(\frac{\partial N}{\partial y})^T]dxdy \qquad 2.48$$

$$[K_2] = \frac{1}{c}\int_{S_2} (N)(N)^T d\ell \qquad 2.49$$

$$[K_3] = \frac{1}{g}\int_{S_3} (N)(N)^T d\ell \qquad 2.50$$

$$(P) = \int_{S_1} V_n(N)d\ell \qquad 2.51$$

The matrices $[K_1]$, $[K_2]$, and $[K_3]$ are symmetric and banded. A Cholesky solution technique capable of handling complex numbers is employed to solve for (ϕ).

Figure 2 shows the finite element mesh for the lower frequencies of a rectangular breakwater. The mesh has 317 nodes, 88 elements, and a half bandwidth of 32. The mesh is finest near the body and along the free surface where the highest velocity gradients are expected. The quadratic isoparametric element has a linear variation of velocity. About eight elements per wavelength are required on the free surface to accurately predict wave heights and phase relations at the radiation boundary. As a result the mesh shown is only good for $B/\lambda<0.5$.

CHAPTER 3

MOORING ANALYSIS

3.1 Introduction

For the mooring analysis it is assumed that the forces on the breakwater are of two parts; a steady drift force, which may include steady wind and current forces, and time-varying forces with the same frequency as the incident wave. Similarly, the response of the breakwater is assumed to consist of a static response to the drift force plus a dynamic response to the time-varying forces. The static response is found by applying the equilibrium equations for a catenary cable. This analysis yields the equilibrium configuration for the dynamic analysis. In the dynamic analysis the mooring cables are modelled by a series of straight, pin-ended bars and the stiffness, mass, and damping matrices for the combined mooring-breakwater system are assembled. Solution of these equations gives the motions of the breakwater. Since the drift force associated with these motions is in general not the same as the drift force assumed in the static analysis, the procedure is repeated until convergence on the drift force is achieved.

3.2 Static Analysis

Figure 3 shows a typical breakwater mooring system. The moorings consist of pairs of chains or cables at right angles to the axis of the breakwater spaced at a distance Z along the breakwater. The anchors are spaced a distance S apart. It is assumed that the water depth is constant between the anchors.

For slack moorings, the stiffness of the moorings is much less than the hydrostatic stiffness of the breakwater in heave or roll. Therefore, it is assumed for the static analysis that the breakwater is fixed in the heave and roll degrees of freedom and that the drift force causes a displacement in the sway mode only. The purpose of the static analysis is then to find the horizontal position of the breakwater with respect to the anchors that results in equilibrium between the horizontal forces in the mooring cables and the drift force.

Two possible configurations for a mooring cable are given in Figure 4. The cable has a buoyant weight of w_c per unit length, a cross-sectional area A, and an elastic modulus E. The unstretched initial length of the cable is C, the rise is h, and the span L. The horizontal force at the upper end of the cable to maintain equilibrium is H. The subscripts 1 and 2 refer to the seaward and shoreward cables respectively.

Figure 4(a) shows a cable that is raised above the sea bed for its entire length. Equilibrium for the cable yields[24]

$$\{(C + \Delta)^2 - h^2\}^{\frac{1}{2}} = \frac{2H}{w_c}\sinh\left(\frac{w_c L}{2H}\right) \qquad 3.1$$

where Δ is the elastic elongation of the cable given by

$$\Delta = \frac{HL}{AE}\left\{\frac{w_c h^2}{2HL}\coth\left(\frac{w_c L}{2H}\right) + \frac{1}{2} + \frac{H}{2w_c L}\sinh\left(\frac{w_c L}{H}\right)\right\} \qquad 3.2$$

Equation 3.1 can be written as

$$\Delta = [(\frac{2H}{w_c}\sinh(\frac{w_c L}{2H}))^2 + h^2]^{\frac{1}{2}} - C \qquad 3.3$$

Equating the right hand sides of Equations 3.2 and 3.3 gives an equation which can be solved iteratively to give the horizontal force H for a given span L. The slope of the cable at the anchor can be calculated from

$$\tan\theta = \frac{w_c}{2H}[h \coth(\frac{w_c L}{2H}) - (C + \Delta)] \qquad 3.4$$

If $\tan\theta < 0$, the cable lies along the sea bed for part of its length as shown in Figure 4(b). The raised span L_s is given by

$$L_s = \frac{H}{w_c}\cosh^{-1}(\frac{hw_c}{H} + 1) \qquad 3.5$$

The initial length of the catenary is

$$C_s = C - (L - L_s) \qquad 3.6$$

Equations 3.2 and 3.3 can be applied by replacing Δ, L, and C with Δ_s, L_s, and C_s respectively. The same iterative solution is used but a new raised span must be calculated for each trial value of H. The total elongation of the cable, including the portion on the sea bed is

$$\Delta = \Delta_s + \frac{H}{AE}(L - L_s) \qquad 3.7$$

Since the horizontal force cannot be expressed explicitly as a function of the span an iterative procedure must be used to find the equilibrium position of the breakwater. A trial value for the span of the seaward cable (L_1) is chosen and the span of the shoreward cable (L_2) is calculated. If $L_2 + h_2 < C_2$, the shoreward cable hangs straight down and is neglected in further calculations. The horizontal force in each cable is

calculated and horizontal equilibrium

$$\Sigma F = F_D Z + H_2 - H_1 \qquad 3.8$$

is checked. The span of the seaward cable is then adjusted according to the sign of ΣF and new horizontal cable forces are calculated. The procedure is repeated until $\Sigma F = 0$ within the desired tolerance.

Once horizontal equilibrium of the breakwater is satisfied, the location of any point on the catenary can be determined. The equation of the catenary is

$$y = \frac{H}{w_c} \cosh\left(\frac{w_c x}{H} + A\right) + B \qquad 3.9$$

where

$$A = \sinh^{-1}\left(\frac{w_c h}{2H \sinh\left(\frac{w_c L}{2H}\right)}\right) - \frac{w_c L}{2H} \qquad 3.10$$

$$B = -\frac{H}{w_c}\cosh(A) \qquad 3.11$$

x and y are in the local coordinate system for the cable. In this system the origin is at the anchor and the coordinate of the upper end of the cable is (L,h). In the case where the cable lies on the sea bed, the origin is at the point of tangency with the sea bed and L is replaced by L_s. The tension in the cable can be calculated from

$$T = H\left(1 + \left(\frac{\partial y}{\partial x}\right)^2\right)^{\frac{1}{2}} \qquad 3.12$$

3.3 Dynamic Analysis

The dynamic analysis of the combined mooring-breakwater system uses the matrix stiffness method to assemble the equations of motion of the system. The cables are modelled by a series of straight, pin-ended bars and the breakwater is modelled by a rigid frame connecting the cables to the breakwater degrees of freedom.

The first step in the dynamic analysis is to discretize the system. Figure 5 shows a typical discretized model. For clarity, the figure shows four bar elements per cable while in practice, eight or more elements are used. The static analysis gives the equations of the catenaries in terms of local coordinates for the cables. For n segments per cable, the coordinates of n+1 nodes per cable must be calculated. One node is at the anchor and another is at the point of attachment to the breakwater. If the cable lies partly on the sea bed, a node is placed at the point of tangency. The remaining intermediate nodes are placed such that there is an equal change in slope between adjacent segments. The coordinates of these nodes are then transformed into the global coordinate system. The global x-axis is at the still water level and positive in the direction of wave propogation. The global y-axis is at the centre of buoyancy of the body when in equilibrium with the drift force and positive upward. The average initial tension in each segment is calculated by averaging the tensions at the ends of the element.

A description of the matrix stiffness method may be found in Refs. (22) and (25). The assembly of the element matrices into the structure matrix and the solution of the matrix equation is

standard for plane-frame problems, therefore only the cable element will be described here.

Stiffness Matrix

The structure shown in Figure 5 is unstable unless a stability function is included in the element stiffness matrix. The stability function represents the resistance to lateral displacement provided by the initial tension in the cable. Figure 6(a) shows a cable element in the local coordinate system. The element has a length L, cross-sectional area A, elastic modulus E, and initial tension T. The four degrees of freedom associated with each element are shown. The force-displacement relation for the element is of the form

$$[k](\delta) = (F) \qquad 3.13$$

where [k] is the element stiffness matrix, (δ) is the vector of nodal displacements, and (F) is the vector of nodal forces. Applying a displacement to each of the degrees of freedom in turn and calculating the forces required for equilibrium gives the element stiffness matrix [k]. A unit axial elongation (Fig. 6(b)) yields the axial stiffness terms

$$\begin{aligned} k_{11} &= -k_{31} = AE/L \\ k_{21} &= k_{41} = 0 \end{aligned} \qquad 3.14$$

A unit lateral displacement (Fig. 6(c)) yields the stability terms

$$\begin{aligned} k_{22} &= -k_{42} = T/L \\ k_{12} &= k_{14} = 0 \end{aligned} \qquad 3.15$$

Repeating for displacements in degrees of freedom 3 and 4 gives the complete element stiffness matrix

$$[k] = \frac{1}{L}\begin{bmatrix} AE & 0 & -AE & 0 \\ 0 & T & 0 & -T \\ -AE & 0 & AE & 0 \\ 0 & -T & 0 & T \end{bmatrix} \qquad 3.16$$

It is assumed here that the axial tension is constant for an element. In fact, the tension will vary with time when the dynamic loads are applied, but this is neglected for the linear analysis.

Mass Matrix

The element mass matrix is found in the same way as the element stiffness matrix, except that an acceleration rather than a displacement is applied at each degree of freedom. There are two masses associated with the element. For axial acceleration, the actual mass of the element is used. For lateral acceleration, the virtual mass, which is the sum of the actual and added masses is used. The added mass for the cables is assumed to be independent of frequency. For a circular cross-section the added mass is taken as the mass of fluid displaced by the cable. For an actual mass per unit length m and a virtual mass per unit length m', the element mass matrix is

$$[m] = L\begin{bmatrix} m/3 & 0 & m/6 & 0 \\ 0 & m'/3 & 0 & m'/6 \\ m/6 & 0 & m/3 & 0 \\ 0 & m'/6 & 0 & m'/3 \end{bmatrix} \qquad 3.17$$

A check on the above mass and stiffness matrices in which the natural frequencies and mode shapes calculated by the matrix stiffness method are compared to an analytic solution is contained in Appendix B.

Damping Matrix

The damping force on the cable is made up of the drag force of the fluid and the structural damping of the cable itself. The drag force per unit length of cable is given by

$$F = \frac{1}{2}\rho C_D D_c v|v| \qquad 3.18$$

where v is the normal velocity of the cable, C_D is the drag coefficient, and D_c is the diameter of the cable. The drag coefficient is a function of Reynold's Number (Re) and the Keulegan-Carpenter Number (K_c). Unlike the breakwater body motions for which the Keulegan-Carpenter Number was sufficiently small that drag could be neglected, the cable displacements are large compared to the diameter fo the cable. Sarpkaya[26] has found that for a circular cylinder with $K_c > 30$, C_D is independent of K_c and approximately equal to 1.2. C_D is also nearly independent of Reynold's number for the high values of Re at which the cables operate.

The drag force is proportional to velocity squared while for linear equations of motion the damping must be proportional to velocity. The drag force can be linearized for simple harmonic motion. For an amplitude of motion δ, the drag force can be written as

$$F = \frac{1}{2}\rho C_D D_c (\omega\delta)^2 \cos(\omega t)|\cos(\omega t)| \qquad 3.19$$

Expanding $\cos(\omega t)|\cos(\omega t)|$ as a Fourier series and retaining only the linear term gives

$$F \simeq \frac{4}{3\pi} C_D D_c \omega\delta v \qquad 3.20$$

which is a linear function of velocity. Integrating Equation 3.19 and the linear approximation Equation 3.20 over one cycle yields

the work done by each force for a given amplitude of displacement. The work calculated from the linear approximation is about 1.08 times the work calculated from Equation 3.19.

The structural damping can be assumed to be Coulomb or friction damping due to interaction between the various elements of the cable or chain. Ramberg and Griffin[27] have measured the log decrement of the free vibrations of a slack cable in air. The Coulomb damping force can be calculated from the log decrement by

$$F_c = \frac{\omega_n^2 m \delta_f}{4} \Delta \qquad 3.21$$

where F_c is the Coulomb damping force, ω_n is the natural frequency of vibration, Δ is the log decrement and δ_f is the amplitude of vibration at which Δ is measured.

For the 5/8" diameter cable studied by Ramberg and Griffin, the damping force at low cable tensions is of the order 10^{-2} lb/ft. For the same cable, with an amplitude of motion of 30 times the cable diameter and a frequency of 3 rad/sec, the average fluid damping force from Equation 3.20 is of order 1 lb/ft. Thus the structural damping of the cable is neglected when calculating the damping matrix of the cable element.

Since the amplitude δ is not known in Equation 3.20, the dynamic analysis is done first with no damping and the resulting lateral amplitudes are used to calculate the damping force for the next iteration. The procedure is repeated until convergence on δ is achieved. Calculated values of δ/D_c indicate that K_c is in the range 20 to 100.

The element damping matrix can be found by applying a unit

velocity at each degree of freedom and using Equation 3.20 to find the associated forces. The resulting damping matrix is

$$[b] = L \begin{bmatrix} 0 & 0 & 0 & 0 \\ 0 & d/3 & 0 & d/6 \\ 0 & 0 & 0 & 0 \\ 0 & d/6 & 0 & d/3 \end{bmatrix} \qquad 3.22$$

where

$$d = \frac{4}{3\pi}\rho C_D D_c \omega\delta \qquad 3.23$$

and δ is the average lateral amplitude of the element.

Energy Balance

The cable damping is the only means of dissipating energy in the system. The rate of energy dissipation is

$$W_D = \frac{\omega}{2\pi}\int_0^L \int_0^{\frac{2\pi}{\omega}} F_D v\,dt\,d\ell \qquad 3.24$$

Using Equation 3.20 and replacing v by $\omega\delta\cos\omega t$ gives

$$W_D = \frac{2}{3\pi}\omega^3\rho C_D D_c \int_0^L \delta^3 d\ell \qquad 3.25$$

For an element, assuming a linear variation of displacements between the ends of the element

$$\int_0^L \delta^3 d\ell = \frac{L}{4}(\delta_2{}^3 + \delta_2{}^2\delta_4 + \delta_2\delta_4{}^2 + \delta_4{}^3) \qquad 3.26$$

where δ_2 and δ_4 are the lateral displacements of the ends of the element. For two cables of n segments each

$$W_D = \sum_{i=1}^{2n} \frac{2}{3\pi}\omega^3\rho C_D D_c \frac{L}{4}(\delta_2{}^3 + \delta_2{}^2\delta_4 + \delta_2\delta_4{}^2 + \delta_4{}^3)_i \qquad 3.27$$

This rate of energy dissipation must equal the difference between the rate of energy transfer into the fluid region and the rate of energy transfer out of the fluid region. The rate of energy

transfer per unit width of wave is

$$P = \frac{\rho g h^2}{8} c_g \qquad 3.28$$

where c_g is the group velocity

$$c_g = \frac{1}{2}\left(1 + \frac{2kd}{\sinh(2kd)}\right) c \qquad 3.29$$

For conservation of energy

$$\frac{Z\rho g c_g h_i^2}{8}(1 - K_t^2 - K_r^2) - W_D = 0 \qquad 3.30$$

For an unrestrained body, $W_D = 0$ and the above equation simplifies to Equation 2.39.

Representation of Breakwater

The body of the breakwater is represented by rigid beam elements connecting the points of attachment of the cables to a node at the origin of the coordinate system. This is necessary because the mass, added mass, damping, stiffness, and exciting force matrices from the unrestrained body analysis are expressed for three degrees of freedom at the origin. The rigid beam elements are fixed to the node at the origin and pin-ended at the cable attachment nodes. These beam elements ensure the correct rigid-body displacement relationship between displacements at the origin node and displacements at the upper ends of the cables. There is no mass or damping associated with these elements. The stiffness matrix for beam elements may be found in Ref. 25.

Assembly of Structure Matrices

The element matrices [m], [b], and [k] are assembled into the structure matrices [M], [B], and [K] using the usual techniques of matrix stiffness analysis. Degrees of freedom are assigned to the nodes as shown in Figure 5. The element matrices are transformed into the global coordinate system and added into the structure matrices. The mass, added mass, damping, and stiffness matrices from the unrestrained analysis (Eqn. 2.33) are added at the degrees of freedom of the origin node. The load vector (X) is expanded to match the increased number of degrees of freedom. The only non-zero entries in the load vector are associated with the origin node degrees of freedom as it is assumed that the incident wave forces do not act directly on the cables. Finally, the assumption of simple harmonic motion is applied in order to express velocities and accelerations in terms of displacements. The result is the matrix equation

$$\{-\omega^2 [M] + i\omega [B] + [K]\} (\xi) = (X) \qquad 3.31$$

The matrices [M], [B], and [K] are banded, symmetric, and of order 4n + 3. In addition [K] is positive definite.

The equations are solved by the same complex Cholesky solution used for the fluid finite elements. The resulting displacement vector (ξ) contains both the cable nodal amplitudes and the breakwater amplitudes. The transmission coefficient and a new drift force are calculated from the breakwater amplitudes in the same way as for the unrestrained body.

Figure 7 is a flow chart for the complete solution. The solution for one frequency using a 317 node finite element mesh and 8 elements per cable takes approximately 4 seconds CPU time

on an Amdahl 470 V/6 Model II computer. Of this approximately 3 seconds are required for the finite element solution and one second for the mooring solution. A typical computer plot showing both the equilibrium and instantaneous position of the breakwater and cables is given in Figure 8.

CHAPTER 4

MOTION OF THE UNRESTRAINED BODY

4.1 Added Mass and Damping

The important results of the hydrodynamic analysis of the unrestrained body pertain to the added mass and damping coefficients, the exciting forces, the transmission coefficient, and the drift force. The added mass, damping, and exciting forces appear in the equations of motion of the combined body-mooring system while the transmission coefficient and drift force serve as the basis for determining the effects of the mooring system.

The added mass and damping coefficients and exciting forces for several simple geometries have been calculated according to potential theory and experimentally verified by Vugts[29]. The potential theory results were calculated by the method of Ursell[4]. Since Vugts was interested primarily in ship motions, infinite water depth was assumed and the frequency was described by the dimensionless parameter $\omega\sqrt{(B/2g)}$ where B is the beam of the body. For the case of a floating breakwater, intermediate and shallow depths must be considered which means the frequency is no longer sufficient to describe the wavelength of the incident wave. A more useful dimensionless parameter for

describing frequency is the beam to wavelength ratio B/λ. In this case, a family of added mass and damping curves are produced, each corresponding to a different water depth ratio B/d. In deep water $B/\lambda = (1/\pi)(\omega\sqrt{B/2g})^2$.

The suitability of the finite element method in predicting the motions of the breakwater depends on both the agreement of finite element results with other potential flow solution methods and the agreement of potential theory results with experiment. Figures 9 through 11 compare results for various added mass and damping coefficients and exciting forces for a circular cylinder and a rectangular cylinder with a beam to draught ratio of 4:1. The solid curves correspond to the results of Vugts. The added mass and damping curves are calculated according to potential theory by the method of Ursell. The exciting forces are calculated from the damping coefficients by the relationship given by Newman[6]

$$|X_i|^2 = 2\rho g c_g b_{ii} \qquad 4.1$$

where c_g is the group velocity of the wave train. This is valid only for bodies that are symmetric about x = 0.

The finite element results are presented as points and are seen to correspond closely to the potential theory results of Vugts. Two finite element meshes were required to cover the range of frequencies shown on the graphs. For $0.1 < B/\lambda < 0.5$, the 317 node mesh shown in Figure 2 was used. This was adapted to the circular cylinder by changing only the elements immediately adjacent to the body. The free surface elements of the mesh have a width of B/4, therefore for the shortest wave, there are eight surface elements per wavelength. The mesh extends a distance

2.5B from the body, therefore for the longest wave, the mesh extends $1/4\lambda$ from the body. For $0.5 < B/\lambda < 1.75$, a 315 node mesh was used. The free surface elements have a width of B/10, therefore for the shortest wave there are 5.7 surface elements per wavelength. The mesh extends a distance of B away from the body, therefore for the longest wave, the mesh extends $1/2\lambda$ from the body. Using these two meshes yields added mass and damping coefficients that are generally within 5% of the potential theory values of Vugts. The effect of mesh size on the accuracy of the results has not been studied.

The experimental values of Vugts agree closely with the potential theory results with a few exceptions. At very low frequencies ($B/\lambda < 0.02$) the experimental values are considerably different from the potential theory results. A frequency of $B/\lambda = 0.02$ and a wave steepness of $H/\lambda = 0.01$ corresponds to a Keulegan-Carpenter number of 16 which is in the range where viscous effects are important. $B/\lambda = 0.02$ is below the range of frequencies of interest as the transmission coefficient is nearly unity for such long waves.

Other discrepancies occur in the damping coefficient in roll and in the coupled modes involving roll. The experimental damping coefficient is sometimes much greater than that predicted by potential theory. As a result, predicted roll amplitudes may be too large, particularly near the resonant frequency in roll. Adee[30] suggests using twice the potential theory roll damping in the equations of motion to represent the viscous effects.

4.2 Motion of the Unrestrained Body

The combination of added mass and damping coefficients and exciting forces with the body mass and hydrostatic stiffness gives the equations of motion for the unrestrained body (Eqn. 2.33). These are solved to give the amplitudes of body motion. Figure 12 shows the amplitudes of motion in the heave and sway modes for a circular cylinder. The mass of the cylinder is ρV and the centre of mass is assumed to be at the still water level. Figure 13 shows the corresponding transmission coefficient. Both amplitudes and the transmission coefficient are presented as functions of the beam to wavelength ratio (B/λ). For a circular cylinder, oscillations in the roll mode do not create any disturbance in the fluid so the amplitude of the transmitted wave will depend only on the heave and sway amplitudes and phase angles.

At low frequencies ($B/\lambda < 0.1$) the sway and heave motions are in phase with, and have the same amplitude as, the horizontal and vertical particle excursions respectively. For a deep water wave, the horizontal and vertical amplitudes for a particle at the free surface will be equal to the wave amplitude. Thus the breakwater follows the same circular orbit as the water particles around it and disturbance of the wave train is at a minimum. This results in a transmission coefficient near unity (Fig. 13). Because the incident wave is not greatly disturbed by the breakwater, the finite element solution is not required and a much simpler approximation such as the Froude-Krylov hypotheses[16] can be used to find the forces on the body.

As the frequency of the incident wave increases, the vertical amplitude of body motion increases to a maximum, then decreases while the horizontal amplitude steadily decreases. In addition, a phase angle is introduced between the body displacements and the particle displacements of the incident wave. The disturbance caused to the incident wave by the breakwater increases with frequency and in general the transmission coefficient decreases. It is in this frequency range that the finite element method is useful in finding the potential fields due to wave scattering and body motion.

At high frequencies ($B/\lambda > 1.0$) the heave amplitude approaches zero and the predominant motion is sway. Since the short waves attenuate quickly with depth, very little of the incident wave passes under the body, thus the transmitted wave is produced mainly by the sway motion. This can be checked by considering the incident wave to be completely reflected and the transmitted wave to be completely generated by the horizontal motion of the body. Linear potential theory gives the dynamic pressure on a vertical wall with a reflection coefficient of 1.0 as

$$p = \rho g h_i \frac{\cosh(k(y + d))}{\cosh(kd)} \cos\omega t \qquad 4.2$$

For a wall extending from $y = 0$ to $y = -D$, where D is the draught of the breakwater, and for deep water waves, integrating the pressure over the depth gives the force on the wall as

$$F = \frac{\rho g^2 h_i}{\omega^2}(1 - e^{-kD}) \cos\omega t \qquad 4.3$$

Assuming only one degree of freedom (sway) for the breakwater, the equation of motion becomes

$$(-\omega^2(m + a_{11}) + i\omega b_{11})\xi_1 = F \qquad 4.4$$

Neglecting damping, the sway amplitude $|\xi_1|$ is then

$$|\xi_1| = \frac{\rho g^2 h_i}{\omega^2} \frac{(1 - e^{-kD})}{(m + a_{11})} \qquad 4.5$$

The dashed line of Figure 12 shows the sway amplitude for a circular cylinder calculated from Equation 4.5.

The amplitude of the transmitted wave can be estimated by the wavemaker theory[16]. The height of wave generated by the horizontal motion of a vertical wall is

$$h_t = \frac{4\omega}{g} \int_{-\infty}^{0} U(y) e^{ky} dy \qquad 4.6$$

where the horizontal velocity of the wall is $U(y)\cos\omega t$. Taking $U(y) = \omega|\xi_1|$ for $-D \leq y \leq 0$ and $U(y) = 0$ elsewhere, the transmission coefficient becomes

$$K_t = \frac{4\rho g^2}{\omega^4} \frac{(1 - e^{-kD})^2}{(m + a_{11})} \qquad 4.7$$

Equation 4.7 assumes that none of the incident wave is transmitted beneath the breakwater. This would require a draught of breakwater of at least one-half the wavelength, however it appears that the approximation is good even for smaller ratios of D/λ. The dashed line of Figure 13 indicates the transmission coefficient for a circular cylinder as calculated from Equation 4.7. For $B/\lambda > 1.0$ the approximate solution corresponds closely to the finite element solution. There can be an advantage to using the approximation in that the only finite element result required is the added mass coefficient. For some shapes this coefficient may be known, or it can be estimated by extrapolating the results for lower frequencies. Also, the added mass can be accurately calculated using a finite element grid that is too coarse to

allow calculation of the wave height on the radiation boundary. The wave height depends on the phase relation among the various potential fields at the boundary and a fine grid is required to accurately predict these phase relations.

4.3 Drift Force

The final result of the hydrodynamic analysis is the drift force. According to Maruo[20], the drift force on an unrestrained body is proportional to the square of the reflected wave amplitude. From Equation 2.39, the drift force is thus proportional to $(1 - K_t^2)$. For long wavelengths, where the entire wave is transmitted, the drift force should be near zero. For short wavelengths, where nearly all the wave is reflected, the drift force should approach $\frac{1}{2}\rho g(h_i/2)^2$. Figure 14 shows the drift force, normalized by dividing by $\frac{1}{2}\rho g(h_i/2)^2$ for an unrestrained circular cylinder. The drift force is proportional to the square of the incident wave height while the oscillatory forces are linear functions of the wave height. Thus the drift force is expected to be more important for large wave heights than for small.

CHAPTER 5

EFFECT OF MOORINGS

5.1 Introduction

The solution of the unrestrained motion problem gives the desired pressures, motions, and transmission coefficient for a freely floating body. When considering a floating breakwater, the body of the breakwater is restrained by some type of mooring system and it is desirable to know the effect of the mooring system on the body motions and the forces in the mooring lines.

Yamamoto and Yoshida[13] have considered the problem by modelling the mooring lines as linear springs and including the spring stiffness in the three equations of motion of the unrestrained body. This method has also been suggested by Adee and Martin[14]. The method is useful when considering taut mooring lines since the force-displacement relation for taut cables can be well represented by a linear spring. Also for taut cables, the initial tension in the cables is very much larger than the drift force. Thus the cable stiffness is nearly independent of wave height and frequency.

In practice, slack moorings are generally used to reduce anchor forces and allow for changes in water depth due to tides. Adee and Martin have used the results of the unrestrained analysis

as an approximation of a breakwater with slack moorings.

In this chapter, a typical breakwater section with slack moorings will be analysed using the procedures of Chapters 2 and 3. First, a dimensional analysis will be carried out to determine the important parameters, then the effect of varying some of these parameters will be demonstrated.

5.2 Dimensional Analysis

The inclusion of mooring lines greatly increases the number of variables needed to describe the behavior of the system. For a given body shape the unrestrained motion may be defined in terms of h_i, d, and λ (which specify the incident wave train), ρ, g, and B. In addition, the dispersion relation

$$\omega^2 = gk \tanh(kd) \qquad 5.1$$

is required to relate the wavelength to the frequency of the wave. A dimensional analysis gives for any chosen dependent variable, say h_t,

$$\frac{h_t}{h_i} = fn\left(\frac{B}{d}, \frac{B}{\lambda}, \frac{h_i}{\lambda}\right) \qquad 5.2$$

For deep water ($B/d \to 0$) and small wave heights ($h_i/\lambda \to 0$), h_t/h_i asymptotically approaches a finite value, therefore Equation 5.2 reduces to

$$\frac{h_t}{h_i} = fn\left(\frac{B}{\lambda}\right) \qquad 5.3$$

Thus for deep water and linear waves, the transmission coefficient of an unrestrained body depends only on the geometry of the body and the beam to wavelength ratio. Similar functional dependence exists for other dependent variables such as amplitudes of motion and forces on the body.

In order to completely describe the motions of a breakwater restrained by mooring cables, the additional variables S, Z, and D_c, ρ_c, C, and E for each cable must be specified. ρ_c is the unit weight of the cable. For simplicity, this analysis will assume that both cables are identical and inextensible and thus only the five additional variables S, Z, D_c, ρ_c, and C are required. Combining these with the variables for unrestrained body motion and performing a dimensional analysis yields

$$\frac{h_t}{h_i} = fn\left(\frac{B}{\lambda}, \frac{h_i}{\lambda}, \frac{B}{d}, \frac{S}{d}, \frac{C}{d}, \frac{Z}{B}, \frac{D_c}{B}, \frac{\rho_c}{\rho}\right) \qquad 5.4$$

Again, the wave frequency need not enter Equation 5.4 as the dispersion relation (Eqn 5.1) relates frequency to the wavelength.

The ratio h_t/h_i is the transmission coefficient K_t. As this is a measure of the efficiency of the breakwater, it is chosen here as the representative dependent variable and the effect of other parameters on K_t will be investigated. B/λ is a measure of the frequency of the incident wave. The plot of K_t vs. B/λ shows the range of frequencies for which the breakwater is effective.

h_i/λ is the wave steepness. For a linear analysis such as that of the unrestrained body, the transmission coefficient is independent of the wave steepness. In the mooring analysis, the drift force, initial configuration of the cables, and the cable damping are all non-linear, therefore the transmission coefficient will depend on the wave steepness.

B/d is a measure of the depth of water. In the hydrodynamic analysis, the added mass and damping coefficients and exciting forces depend on the B/d ratio. In particular, the added mass in heave increases for shallow water. Bai[31], and Yamamoto and

Yoshida[13] have found that for depth to draught ratios (d/D) greater than six, infinite depth can be assumed. In the mooring analysis, B/d along with S/d are needed to describe the geometry of the moorings.

The ratio C/d is the scope of the mooring lines. For a given B/d and S/d, the ratio C/d is a measure of the tautness of the cables.

The aspect ratio Z/B is the length of breakwater associated with one set of mooring lines. The mooring lines are described by a dimensionless size parameter D_c/B and their specific gravity ρ_c/ρ.

5.3 Properties of Breakwater

The dimensional analysis indicates there are eight independent parameters affecting the motion of a moored breakwater. For this study only one geometry and three independent parameters, B/λ, h_i/λ, and C/d will be considered.

The general arrangement of the breakwater to be analysed is shown in Figure 15. The breakwater body is rectangular in section with a beam to draught ratio (B/D) of 4.0. The mass of the body is the underwater volume times the density of water. The mass is assumed to be evenly destributed throughout the underwater volume when calculating the centre of gravity and the polar moment of inertia of the body. Thus the moment of inertia of the body about the origin is $\frac{5}{192}\rho B^4$ and the centre of gravity is at (0,-B/8). The additional vertical force due to the mooring cables has been neglected so vertical equilibrium is not satisfied. However, the vertical component of the mooring line tensions is generally less than five percent of the weight of the body for

the breakwater analyzed here. The added mass and damping coefficients in heave and sway for this body are shown in Figure 10.

The frequency range to be studied is $0.05 < B/\lambda < 1.75$. Most variation in K_t occurs within this range. The range of wave steepness considered is $0.01 \leq h_i/\lambda \leq 0.14$. For $h_i/\lambda = 0.01$, the drift force is nearly zero. Also, the lateral amplitude of the cables, and thus the drag is near zero. Therefore, the results for $h_i/\lambda = 0.01$ should correspond to those of a totally linear analysis. $h_i/\lambda = 0.14$ corresponds approximately to the steepest wave in deep water.

The depth ratio B/d is set at 0.2 so that for most of the frequency range studied ($B/\lambda > 0.1$) the wavelength to depth ratio is less than two and deep water can be assumed. This allows comparison of the hydrodynamic coefficients found by the finite element method with the results of Vugts.

A range of C/d values will be studied to show the effect of taut or slack moorings. The remaining parameters are arbitrarily selected to reflect typical conditions for floating breakwaters. These parameters are: $Z/B = 4.0$, $S/d = 5.5$, $D_c/B = 0.0187$, and $\rho_c/\rho = 6.8$. For the above parameters and with $C/d = 3.0$, the total cable weight, assuming a solid circular cross-section, is 6.4% of the weight of the breakwater.

5.4 Effect of Moorings

From Equation 2.35, the velocity potential of the transmitted wave is

$$\phi = \phi_0 + \phi_R + \sum_{j=1}^{3} \xi_j \phi_j \qquad 5.5$$

The transmission coefficient can be written as

$$K_t = \frac{\left|\phi_0 + \phi_R + \sum_{j=1}^{3} \xi_j \phi_j\right|}{|\phi_0|} \qquad 5.6$$

The velocity potentials are functions of the incident wave and the breakwater geometry, therefore any change in the transmission coefficient due to the moorings is the result of a change in the complex amplitudes ξ_j.

Figure 16 shows the transmission coefficient for the rectangular breakwater with five different restraint conditions; free, fixed, sway motion only, heave motion only, and roll motion only. As for the unrestrained circular cylinder discussed in Chapter 4, the response of the rectangular breakwater may be divided into three frequency ranges; low frequency ($B/\lambda < 0.1$), intermediate frequency ($0.1 < B/\lambda < 1.0$), and high frequency ($B/\lambda > 1.0$).

At low frequencies, the transmission coefficient is near unity regardless of the restraint condition. In terms of Equation 5.6, the incident wave potential ϕ_0 predominates at low frequencies.

At intermediate frequencies, the transmission coefficient is highly dependent on the restraint condition. The transmission coefficient is generally highest for the freely floating body and lowest for the fixed body. For the freely floating body there is

a condition of complete transmission at about $B/\lambda = 0.38$. The location of this maximum is extremely sensitive to changes in the location of the centre of gravity of the body. The roll motion only condition also shows a local maximum in the transmission coefficient near $B/\lambda = 0.38$. For the fixed, sway only, and heave only conditions, the transmission coefficient decreases monotonically with increasing B/λ.

At high frequencies only the free and sway only conditions have a non-zero transmission coefficient. This supports the approximation of Section 4.2 that for high frequencies, all the transmitted wave is produced by motion in the sway mode.

Figure 17 shows the transmission coefficient for the breakwater with a typical slack mooring. The parameters are $C/d = 3.0$ and $h_i/\lambda = 0.1$. The fixed and free transmission coefficients are shown for reference. Figures 18 through 20 show the amplitude and phase angle for each mode in both the free and slack moored conditions. The phase angle δ is defined such that the displacement at any time is given by $|\xi_j|\cos(\omega t - \delta)$.

At low frequencies the moorings do not change the amplitude or phase angle of the motions. The body of the breakwater follows the same path as the surrounding water particles, just as for the unrestrained circular cylinder.

At intermediate frequencies, the moorings have little effect on the heave amplitude or phase angle. The moorings significantly reduce the roll amplitude and change the amplitude and phase angle of the sway motion. These changes can be explained by comparing the unrestrained and slack-moored equations of motion (Eqn. 2.33 and Eqn. 3.31). In the heave mode, the

unrestrained body has considerable damping and hydrostatic stiffness. The stiffness and damping in the moorings is small by comparison, thus the moorings have little effect on the heave motion. There is a slight reduction in amplitude near the heave resonant frequency. In the roll mode, the unrestrained body has considerable stiffness but very little damping. This leads to the resonant response shown in Figure 20. The moorings introduce some damping into the system, resulting in a large reduction in roll amplitude near the resonant frequency. There is also a slight change in phase angle at the resonant frequency due to the extra damping. If the moorings were modelled as linear springs, the resonant roll frequency would change but there would be no reduction in maximum roll amplitude.

In the sway mode, the unrestrained body has mass and damping, but no stiffness. The moorings introduce some horizontal stiffness resulting in a large change in phase angle (Fig. 18). The amplitude in sway is also reduced.

The result of the above changes is a general reduction in the transmission coefficient. The full transmission condition at $B/\lambda = 0.38$ is eliminated due to the reduction in resonant roll amplitude. The greatest change in K_t due to the moorings occurs near the middle of the frequency range. Near $B/\lambda = 0.1$ and $B/\lambda = 1.0$ the moorings have little effect.

At high frequencies, the slack-moored transmission coefficient approaches that of the unrestrained body, despite the additional horizontal stiffness provided by the moorings. At high frequencies the mass terms in the equations of motion predominate. Since the breakwater body mass is much greater than

that of the moorings, the slack-moored and unrestrained motions are nearly identical. Thus the short wavelength approximation developed for the unrestrained body can also be applied to a slack-moored body.

Figure 21 shows the transmission coefficient for the slack-moored breakwater for four different values of wave steepness h_i/λ. The wave steepness determines the relative magnitudes of the steady drift force and the time dependent forces. The drift force is proportional to the square of the wave height while the time dependent forces increase linearly with wave height.

For $h_i/\lambda = 0.01$, the drift force is essentially zero. As the drift force increases, the span of the seaward cable increases as does its horizontal stiffness $\partial H_1/\partial L_1$. As well, the span and horizontal stiffness of the shoreward cable decreases. Taking derivatives of the cable equilibrium equation (Eqn. 3.1), it can be shown that both $\partial H/\partial L$ and $\partial^2 H/\partial L^2$ are always positive. For identical cables, the net result of an increase in the drift force will be an increase in the horizontal stiffness of the combined system. The effect of the increase in mooring stiffness is a decrease in the transmission coefficient in the intermediate frequency range. In the high and low frequency ranges, the transmission coefficient is nearly independent of the wave steepness since at these frequencies the mooring stiffness has little effect on K_t. In Figure 21, K_t is seen to decrease with increasing h_i/λ in the intermediate frequency range only.

A similar pattern appears in Figure 22 with the transmission coefficient decreasing with increasing cable tautness.

For $C/d = 3.33$, the shoreward cable is completely slack and is neglected except for waves in the low frequency range where the drift force is near zero. As the cable tautness increases (decreasing C/d) the horizontal and vertical stiffness of the mooring increases and the transmission coefficient is reduced. Again the effect is limited to the intermediate frequency range.

The tension at the upper end of the seaward and shoreward cables for $h_i/\lambda = 0.1$ and $C/d = 3.0$ is given in Figures 23 and 24. The dashed line indicates the cable tension in still water. At low frequencies the reflection coefficient and thus the drift force is near zero. As a result the equilibrium cable tensions are both near their value for still water. As the drift force increases, the equilibrium tension in the seaward cable increases while the shoreward cable tension decreases. At high frequencies, the reflection coefficient approaches unity, but since the tensions are given for constant wave steepness, the height of the reflected wave and the drift force decrease. As a result, the equilibuium tensions approach their still water value.

The dynamic cable tension is greatest at $B/\lambda \simeq 0.35$. This corresponds to the greatest reduction in K_t due to the moorings. At higher frequencies, the dynamic cable tensions approach zero as the amplitudes of body motion approach zero. In the dynamic model it was assumed that the dynamic tension was small compared to the equilibrium tension. In Figure 23 the dynamic tension is for some frequencies larger than the equilibrium tension resulting in a negative minimum cable tension. A better approximation would be to calculate the stability terms in the stiffness matrix according to the actual tension in the cable rather than the

equilibrium tension, however this would require a more complex non-linear dynamic analysis.

The above results are for the specific breakwater described in Section 5.3. Many factors other than the wave steepness and mooring tautness influence the transmission coefficient. These include the shape and location of centre of gravity of the breakwater body, aspect ratio, anchor spacing ratio, and weight of the mooring lines. Typical values were selected for the breakwater analyzed here, but the above results may not be general if other values are selected.

CHAPTER 6

CONCLUSIONS AND FURTHER STUDIES

6.1 Conclusions

A method of analyzing slack-moored floating breakwaters has been presented. The finite element method, previously used to find hydrodynamic coefficients in ship motion problems, can be used to find the velocity potential field around a floating breakwater according to linear theory. The finite element method is not efficient for short wavelengths due to the large number of elements required, however, a simple approximation for the transmission coefficient may be used for short wavelengths.

The mooring analysis may be divided into a non-linear static analysis and a linear dynamic analysis. The second-order drift force on the breakwater is important in the static analysis. The linear dynamic analysis can be achieved using standard plane-frame analysis techniques with the addition of special mass and damping matrices for the cable elements.

The transmission coefficient calculated from the combined body-mooring equations of motion may be quite different from that of the unrestrained body. For the breakwater analyzed, the significant changes in transmission coefficient were confined to frequencies where the beam to wavelength ratio was between

0.1 and 1.0, which covers the usual range of design conditions. At lower frequencies the transmission coefficient was nearly unity, regardless of the type of mooring, while at higher frequencies the transmission coefficient for both the unrestrained and slack-moored breakwaters could be found from the same short wavelength approximation. Very low transmission coefficients could not be achieved at reasonably small beam to wavelength ratios unless motion in the sway mode was eliminated.

Changes in the transmission coefficient due to the moorings can be related to changes in the sway amplitude and phase angle, and the roll amplitude. Heave amplitude and phase angle are not significantly affected by the moorings.

The combined body-mooring analysis is non-linear so the transmission coefficient is dependent on wave steepness. The transmission coefficient tends to decrease with increasing wave steepness due to an increase in the stiffness of the moorings. Increasing the tautness of the moorings also tends to decrease the transmission coefficient.

6.2 Further Studies

Further studies in slack-moored floating breakwaters could be made in several areas. As shown in Section 5.2, there are many parameters that influence the transmission coefficient. Only a few have been considered here. The effect of body geometry, centre of gravity, cable density, anchor spacing, and other factors could be examined. The computer program developed here can be used to investigate theoretically such factors, and comparison could be made with experimental results.

The present analysis is for a monochromatic wave. For design purposes it is desirable to obtain a transmitted wave spectrum and extreme mooring forces for a given incident wave spectrum. The non-linear nature of the response means that the transfer function approach can not be used.

The incident wave has been assumed to be normal to the breakwater. An oblique wave would create a simple harmonic variation of wave forces along the axis of the breakwater. This could reduce the amplitude of motion of the breakwater. The finite element solution for an oblique wave interacting with a horizontal freely-floating cylinder has been presented by Bai[32]. This could be extended to the complete breakwater analysis.

BIBLIOGRAPHY

1 Adee, Bruce H. "Operational Experience with Floating Breakwaters", Marine Technology, vol. 14, no. 4, Oct. 1977, pp. 379-386.

2 Dean, W. R. "On the reflection of surface waves by a submerged plane barrier", Proc. Cambridge Phil. Soc., 41, 1945, pp. 231-238.

3 Ursell, F. "Effect of a fixed barrier on surface waves in deep water", Proc. Cambridge Phil. Soc., 43, 1947, pp. 374-382.

4 Ursell, F. "On the heaving motion of a circular cylinder on the surface of a fluid", Q. J. Mech. Math., vol. 2, 1949, pp. 218-231.

5 John, F. "On the motion of floating bodies", Comm. Pure Applied Math., vol. 2, 1949, pp. 13-57.

6 Newton, R. E. "Finite Element Analysis of Two-dimensional Added Mass and Damping", Finite Elements in Fluids, ed. Gallagher, R. H., Oden, J. T., Taylor, C., and Zienkiewicz, O. C., New York, Wiley, 1975, vol. 1, pp. 219-232.

7 Bai, K. J. "A Variational Method in Potential Flows with a Free Surface", Report No. NA 72-2, University of California, Berkeley, College of Engineering, 1972.

8 Chen, H. S. and Mei, C. C. "Oscillations and wave forces in a man made harbour in the open sea", Proc. 10th Symp. Naval Hydrodynamics, Cambridge, Mass., 1974, pp. 573-596.

9 Bettess, P. and Zienkiewicz, O. C. "Diffraction and Refraction of Surface Waves Using Finite and Infinite Elements", Int. Journal for Numerical Methods in Engineering, vol. 11, 1977, pp. 1272-1290.

10 Mei, Chiang C. and Black, Jared L. "Scattering of Surface Waves by Rectangular Obstacles in Waters of Finite Depth", J. Fluid Mech., vol. 38, 1969, pp. 499-511.

11 Takano, K. "Effects d'un obstacle parallelepipedique sur la propogation de la houle", Houille Blanche, 15, p. 247.

12 Nichols, B. D. and Hirt, C. W. "Numerical Calculation of Wave Forces on Structures", Proc. 15th Coastal Engineering Conference, 1975, p. 2254.

13 Yamamoto, Tokuo and Yoshida, Akinori. "Elastic Moorings of Floating Breakwaters", 7th Int. Harbour Congress, Antwerp, 1978.

14 Adee, Bruce H. and Martin, W. "Theoretical Analysis of Floating Breakwater Performance", Proc. 1974 Floating Breakwater Conf., University of Rhode Island, Marine Technical Report Series #24, pp. 21-39.

15 Remery, G. F. M. and van Oortmerssen, G. "The Mean Wave, Wind, and Current Forces on Offshore Structures and their Role in the Design of Mooring Systems", 5th OTC, Paper OTC 1741, 1973.

16 Newman, J.N., Marine Hydrodynamics, Cambridge, Mass., MIT Press, 1977, pp. 237-311.

17 Garrison, C. J. "Hydrodynamics of large objects in the sea, Part I, Hydrodynamic analysis", J. Hydronautics, vol. 8, no. 1, 1974, pp. 5-12.

18 Wehausen, John V. "The Motion of Floating Bodies", Ann. Review of Fluid Mechanics, vol. 3, 1971, pp. 237-268.

19 Bearman, P. W., Graham, J. M. R. and Singh, S. "Forces on cylinders in harmonically oscillating flow", Symp. on Mechanics of Wave-incuced Forces on Cylinders, Bristol, 1978.

20 Maruo, Hajime. "The Drift of a Body Floating on Waves", J. Ship Research, vol. 4, 1960, pp. 1-10.

21 Longuet-Higgins, M. "The mean forces exerted by waves on floating or submerged bodies with applications to sand bars and wave power machines", Proc. Royal Soc. London A. vol. 352, 1977, pp. 463-480.

22 Zienkiewicz, O. C., The Finite Element Method in Engineering Science, 2nd ed., London, McGraw-Hill, 1971

23 Segerlind, L. J., Applied Finite Element Analysis, New York, Wiley, 1976.

24 Dean, D. L. "Static and Dynamic Analysis of Guy Cables", Trans. ASCE, vol. 127, part II, 1962, pp. 382-402.

25 Coates, R. C., Coutie, M. G. and Kong, F. K., Structural Analysis, New York, Wiley, 1972.

26 Sarpkaya, T. "Forces on Cylinders and Spheres in Sinusoidally Oscillating Fluid", Trans. ASME J. Appl. Mech., vol. 42, March 1975, pp. 32-37.

27 Ramberg, Steven E. and Griffen, Owen M. "Free Vibrations of Taut and Slack Marine Cables, Journal of the Structural Division, ASCE, vol. 103, no. ST11, Nov. 1977, pp. 2079-2092.

28 Irvine, H. M. and Caughey, T. K. "The linear theory of free vibrations of a suspended cable", Proc. Royal Soc. Lond. A. vol 341, 1974, pp. 299-315.

29 Vugts, J. H. "The hydrodynamic coefficients for swaying, heaving and rolling cylinders in a free surface", International Shipbuilding Progress, 15, no. 167, July 1968, pp. 251-276.

30 Adee, Bruce H. "Floating Breakwater Performance", Proc. 15th Coastal Engineering Conference, 1975, p. 2777.

31 Bai, K. J. "Added Mass of 2-D Cylinders in Water of Finite Depth", J. Fluid Mechanics, vol. 81, 1977, p. 85.

32 Bai, K. J. "Diffraction of Oblique Waves by an Infinite Cylinder", J. Fluid Mechanics, vol. 68, 1975, p. 513.

APPENDIX A

THE QUADRATIC ISOPARAMETRIC ELEMENT

The quadratic isoparametric element used to solve the boundary-value problem can represent a quadratic geometric boundary shape and a quadratic variation in the velocity potential (ϕ). Since the velocity of the fluid is the first derivative of the potential, a linear variation of velocity across an element can be represented. The velocity potential is continuous across element boundaries while the velocity is not. The element is described in detail by Zienkiewicz[22].

Figure A-1 shows both the global and transformed elements. The element in the global x-y system, which is in general any quadrilateral with straight or parabolic edges, is transformed into the much simpler element in the s-t coordinate system to facilitate integration. The transformations are

$$x = \sum_{i=1}^{8} N_i x_i$$

$$y = \sum_{i=1}^{8} N_i y_i \qquad \text{A1}$$

$$\phi = \sum_{i=1}^{8} N_i \phi_i$$

where (x_i, y_i) is the coordinate of the ith node in the x-y

coordinate system and ϕ_i is the value of ϕ at the ith node. The quadratic shape functions are

$$\begin{aligned}
N_1 &= -(1 - s)(1 - t)(1 + s + t)/4 \\
N_2 &= -(1 + s)(1 - t)(1 - s + t)/4 \\
N_3 &= -(1 + s)(1 + t)(1 - s - t)/4 \\
N_4 &= -(1 - s)(1 + t)(1 + s - t)/4 \\
N_5 &= (1 - s^2)(1 - t)/2 \\
N_6 &= (1 - t^2)(1 + s)/2 \\
N_7 &= (1 - s^2)(1 + t)/2 \\
N_8 &= (1 - t^2)(1 - s)/2
\end{aligned} \qquad \text{A2}$$

From Equation 2.48 the element matrix to be calculated is

$$[k] = \int_{\Omega_e} [(\frac{\partial N}{\partial x})(\frac{\partial N}{\partial x})^T + (\frac{\partial N}{\partial y})(\frac{\partial N}{\partial y})^T]dxdy \qquad \text{A3}$$

The shape functions N_i are functions of the local coordinates s and t. Since x and y can be expressed as functions of s and t

$$\begin{bmatrix} \frac{\partial N_i}{\partial s} \\ \frac{\partial N_i}{\partial t} \end{bmatrix} = \begin{bmatrix} \frac{\partial x}{\partial s} & \frac{\partial y}{\partial s} \\ \frac{\partial x}{\partial t} & \frac{\partial y}{\partial t} \end{bmatrix} \begin{bmatrix} \frac{\partial N_i}{\partial x} \\ \frac{\partial N_i}{\partial y} \end{bmatrix}$$

$$= [J] \begin{bmatrix} \frac{\partial N_i}{\partial x} \\ \frac{\partial N_i}{\partial y} \end{bmatrix} \qquad \text{A4}$$

Inverting

$$\begin{bmatrix} \frac{\partial N_i}{\partial x} \\ \frac{\partial N_i}{\partial y} \end{bmatrix} = [J]^{-1} \begin{bmatrix} \frac{\partial N_i}{\partial s} \\ \frac{\partial N_i}{\partial t} \end{bmatrix} \qquad \text{A5}$$

Thus at any point in the element the desired column vectors $(\partial N/\partial x)$ and $(\partial N/\partial y)$ can be calculated. Integration over the domain of the element is done numerically using Gaussian

quadrature. The expression

$$[f(s,t)] = \left(\frac{\partial N}{\partial x}\right)\left(\frac{\partial N}{\partial x}\right)^T + \left(\frac{\partial N}{\partial y}\right)\left(\frac{\partial N}{\partial y}\right)^T \qquad \text{A6}$$

is evaluated at nine points in the region and the sum

$$[k] = \sum_{i=1}^{3} \sum_{i=1}^{3} W_i W_j [f(s_i, t_j)] |J| \qquad \text{A7}$$

is calculated where

$$\begin{aligned} s_1 &= t_1 = -0.7745967 \\ s_2 &= t_2 = 0.0 \\ s_3 &= t_3 = +0.7745967 \\ W_1 &= W_3 = 0.5555556 \\ W_2 &= 0.8888889 \end{aligned}$$

The boundary integrals are calculated in a similar manner. On the prescribed velocity boundary, the boundary integral is

$$(P)_e = \int_{S_{1e}} V_n (N) d\ell \qquad \text{A8}$$

The prescribed velocity is of the form

$$\underline{V} = V_x \underline{i} + V_y \underline{j} \qquad \text{A9}$$

therefore it is necessary to find the normal to the element boundary in order to calculate the normal velocity. Considering the boundary containing nodes 1,5, and 2, an outward normal to the boundary is

$$\underline{n} = \sum_{i=1}^{8} \frac{\partial N_i}{\partial s} y_i \underline{i} - \sum_{i=1}^{8} \frac{\partial N_i}{\partial s} x_i \underline{j} \qquad \text{A10}$$

The normal velocity is then

$$V_n = \frac{\underline{V} \cdot \underline{n}}{|\underline{n}|} \qquad \text{A11}$$

Again numerical integration is used and the expression

$$[g(s)] = V_n(N) \qquad \text{A12}$$

is calculated at three integration points on the boundary. The boundary integral is then

$$(P)_e = \sum_{i=1}^{3} W_i [g(s_i)] |\underline{N}| \qquad \text{A13}$$

W_i and s_i are as previously defined.

On the free surface and radiation boundaries, the integral $\int_S (N)(N)^T d\ell$ must be calculated. This is done in the same way as the prescribed velocity boundary but with the matrix $(N)(N)^T$ replacing the vector $V_n(N)$.

APPENDIX B

FREE CABLE VIBRATIONS

A theory of linear vibrations of a parabolic cable in air has been developed by Irvine and Caughey[28]. Their theory applies to both extensible and inextensible cables with sag to span ratios of 1:8 or less. Ramberg and Griffin[27] have found that the Irvine and Caughey theory can be applied to marine cables if allowance is made for fluid damping and added mass.

According to Irvine and Caughey, the behavior of a suspended cable is described by the dimensionless parameter

$$\lambda^2 = \left(\frac{8d}{L}\right)^2 \frac{L}{\left(\frac{HL_e}{AE}\right)} \qquad \text{B1}$$

where d is the sag, L the span, H the horizontal force in the cable, A the cross-sectional area of the cable, and E the modulus of elasticity. L_e is an effective cable length which for parabolic cables may be approximated by

$$L_e \simeq L\left(1 + 8\left(\frac{d}{L}\right)^2\right) \qquad \text{B2}$$

The dimensionless frequency of vibration is described by the parameter

$$(\beta L)_n = \omega_n L \left(\frac{m}{H}\right)^{\frac{1}{2}} \qquad \text{B3}$$

where ω_n is a natural frequency and m is the mass per unit length

of the cable. For anti-symmetric in-plane modes, the natural frequencies are given by

$$(\beta L)_n = 2n\pi \qquad n=1,2,3.... \qquad \text{B4}$$

For symmetric in-plane modes, the natural frequencies are given by the transcendental equation

$$\tan(\tfrac{1}{2}\beta L) = (\tfrac{1}{2}\beta L) - (\tfrac{4}{\lambda^2})(\tfrac{1}{2}\beta L)^3 \qquad \text{B5}$$

For an inextensible cable, λ^2 is very large and the approximate natural frequencies for symmetric in-plane modes are given by

$$\begin{array}{lll} (\beta L)_1 & 2.86\pi & \\ (\beta L)_2 & 4.92\pi & \\ (\beta L)_n & (2n+1)\pi & n=3,4,5.... \end{array} \qquad \text{B6}$$

The cable model of Chapter 3 was checked against the results of Irvine and Caughey. A cable with a sag to span ratio of 1:10 was selected. The cable was divided into ten equal length segments and the mass and stiffness matrices were assembled. The added mass and damping were set to zero. The resulting equation

$$\{-\omega_n^2[M] + [K]\}(\xi) = (0) \qquad \text{B7}$$

was solved for the natural frequencies ω_n and the mode shapes (ξ) using a library eigenvalue routine. The results are shown in Figure B-1. The non-dimensional frequency βL is shown along with the results of Irvine and Caughey in brackets. For the first four modes, the maximum error in βL is 9%. The error generally increases as the number of elements per wavelength decreases. The maximum 9% error corresponds to four elements per wavelength.

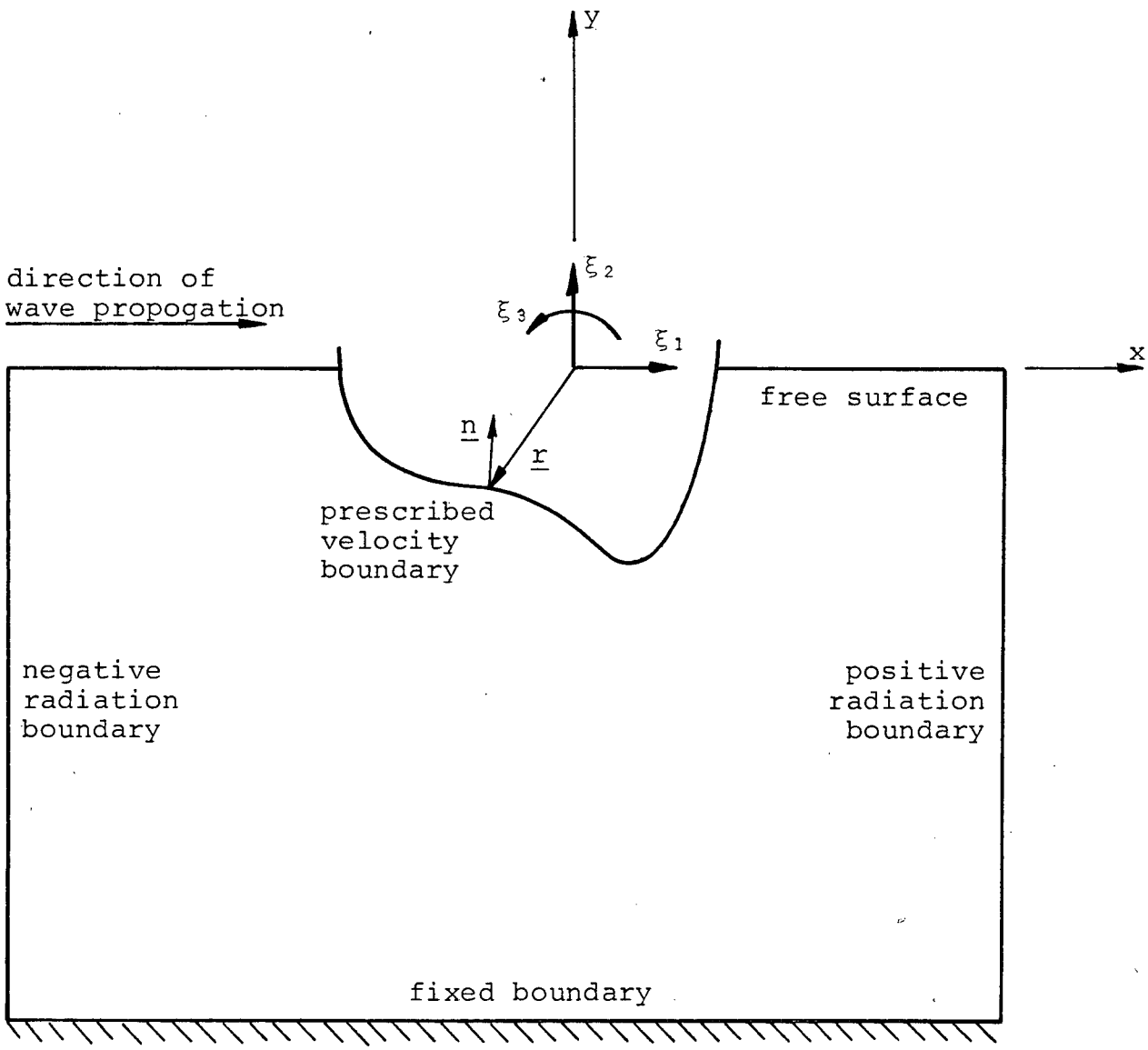

DEFINITION SKETCH - FLUID REGION

FIGURE 1

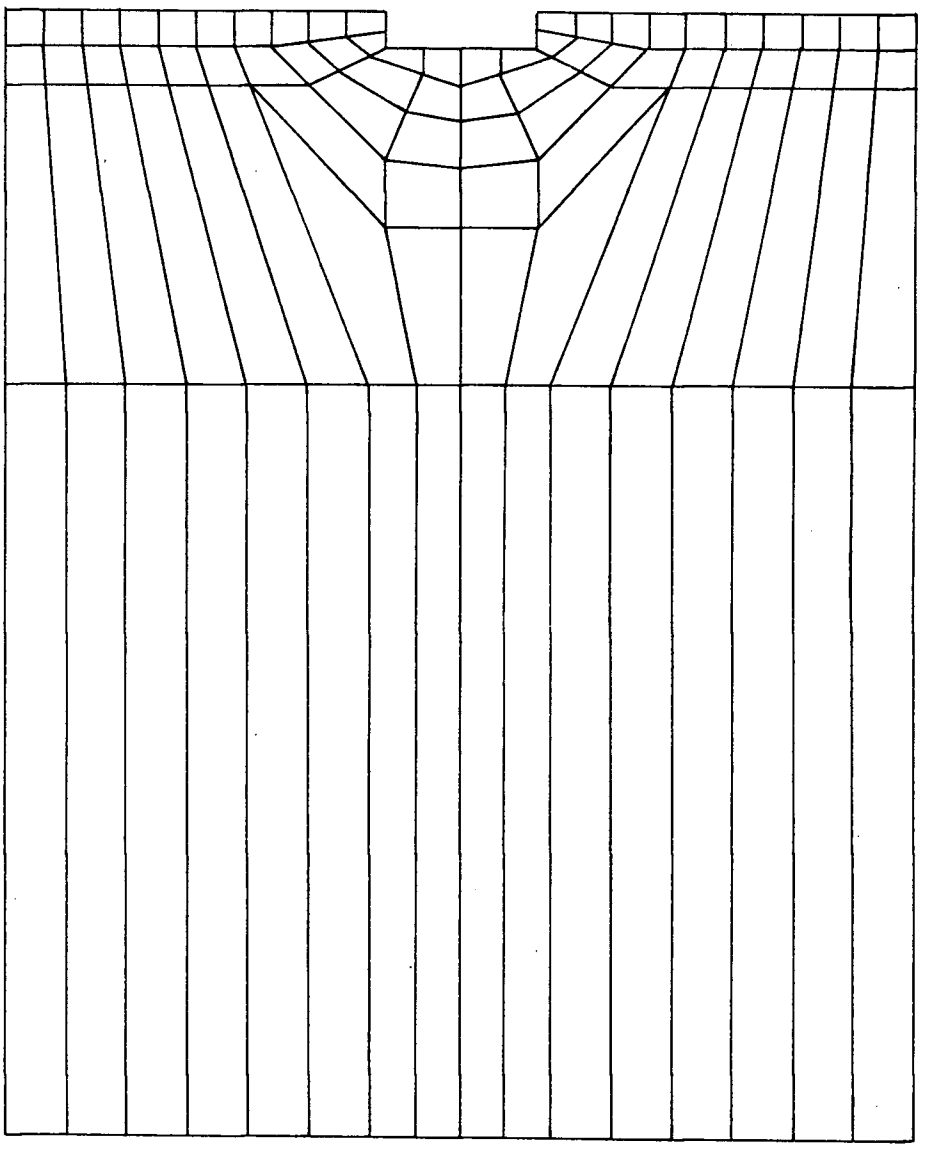

FINITE ELEMENT MESH

FIGURE 2

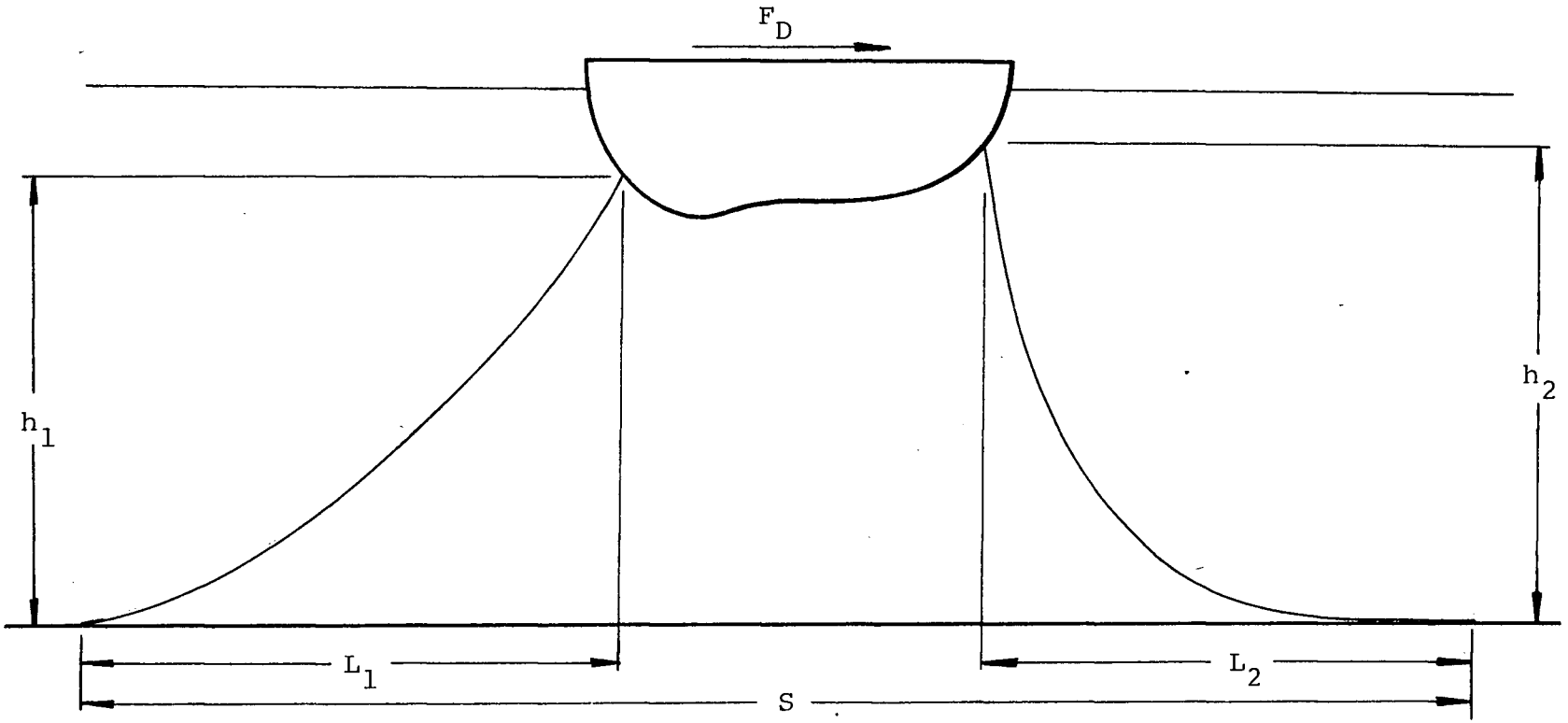

DEFINITION SKETCH - MOORING SYSTEM

FIGURE 3

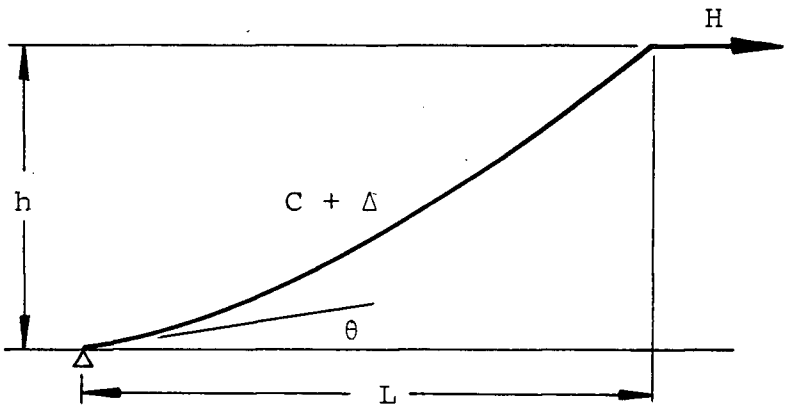

(a) $\theta \geq 0$

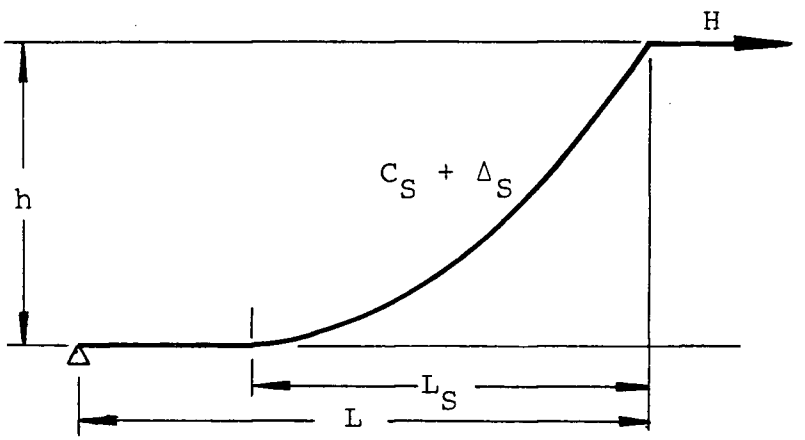

(b) $\theta < 0$

CABLE DEFINITIONS

FIGURE 4

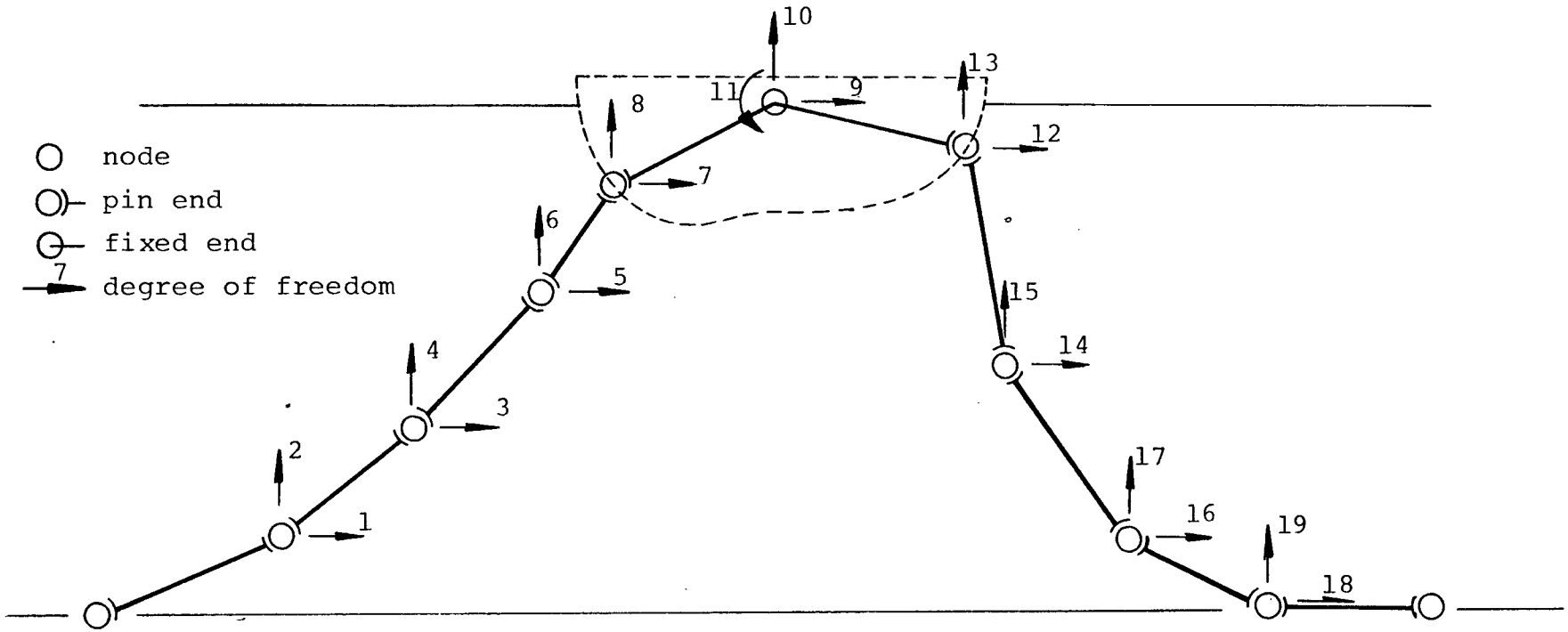

DYNAMIC STRUCTURAL MODEL

FIGURE 5

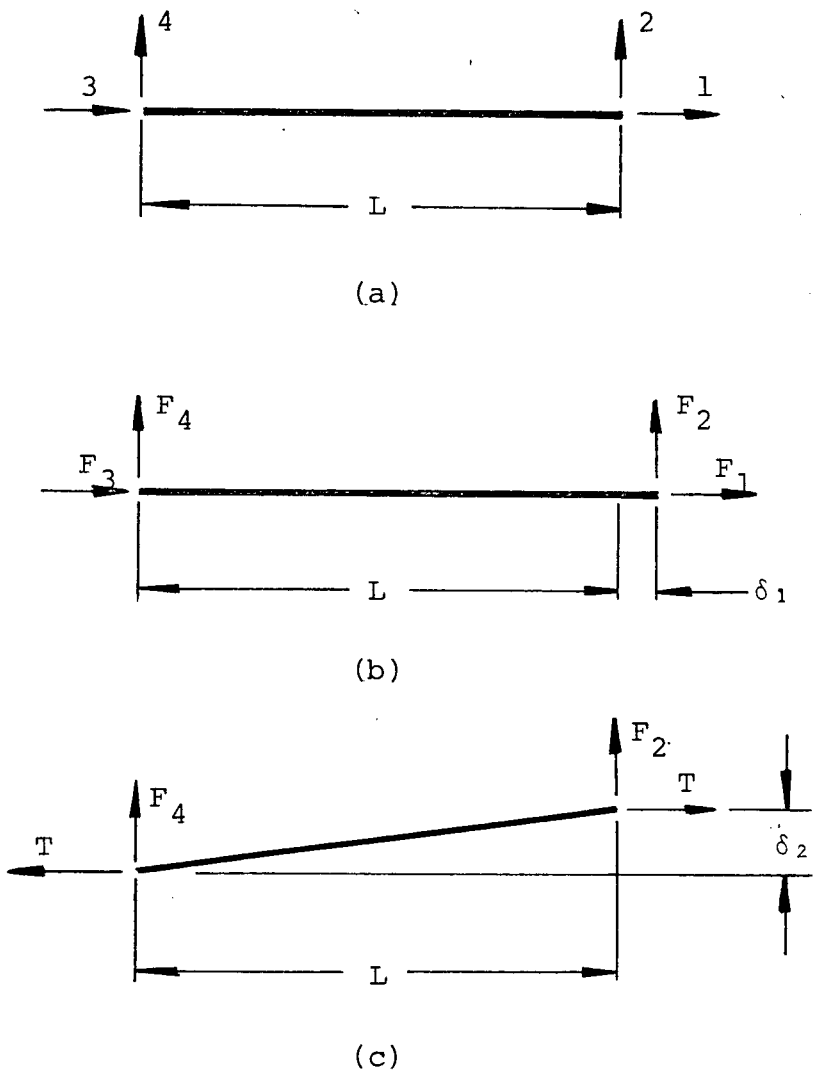

CABLE ELEMENT

FIGURE 6

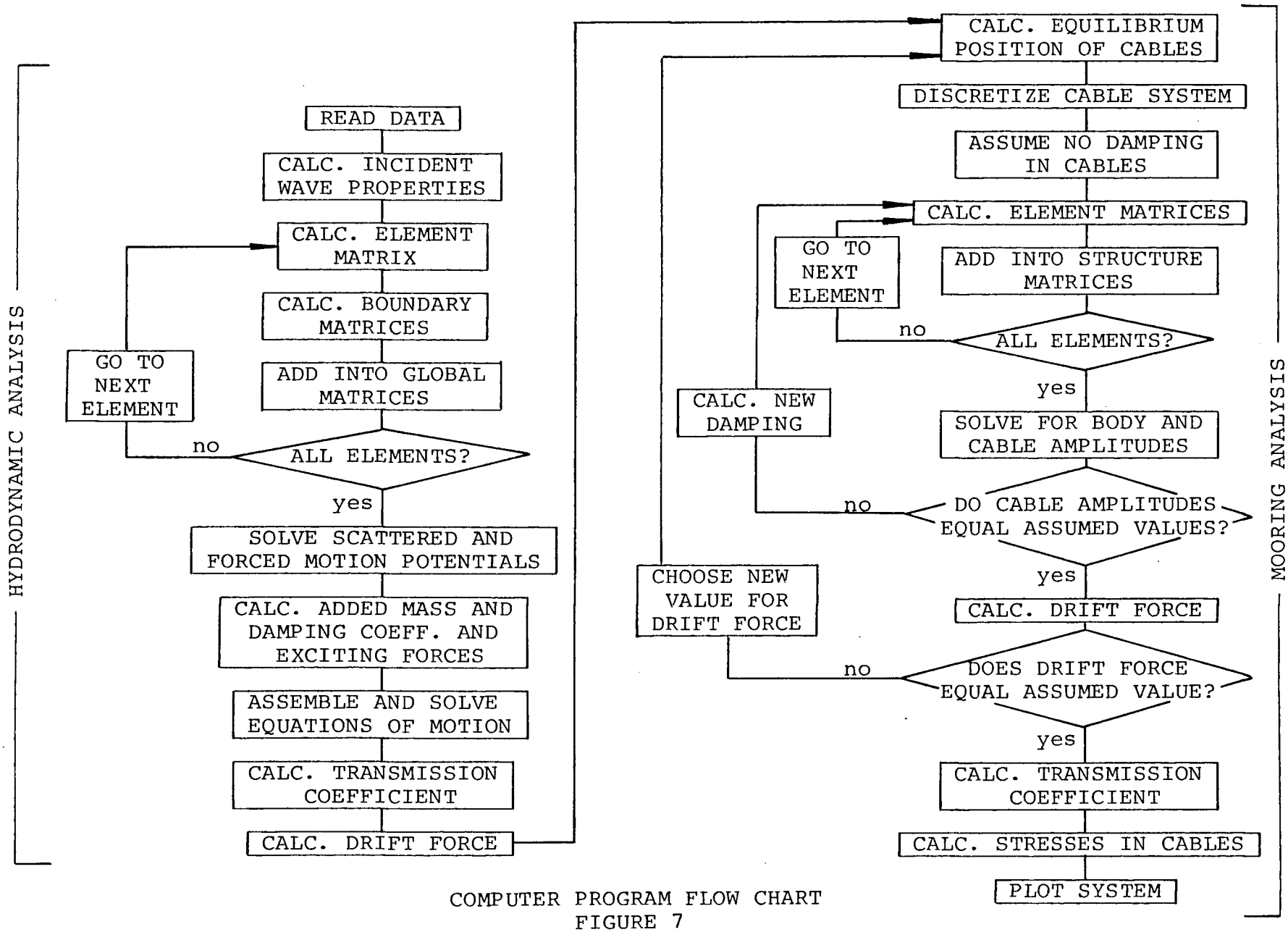

COMPUTER PROGRAM FLOW CHART
FIGURE 7

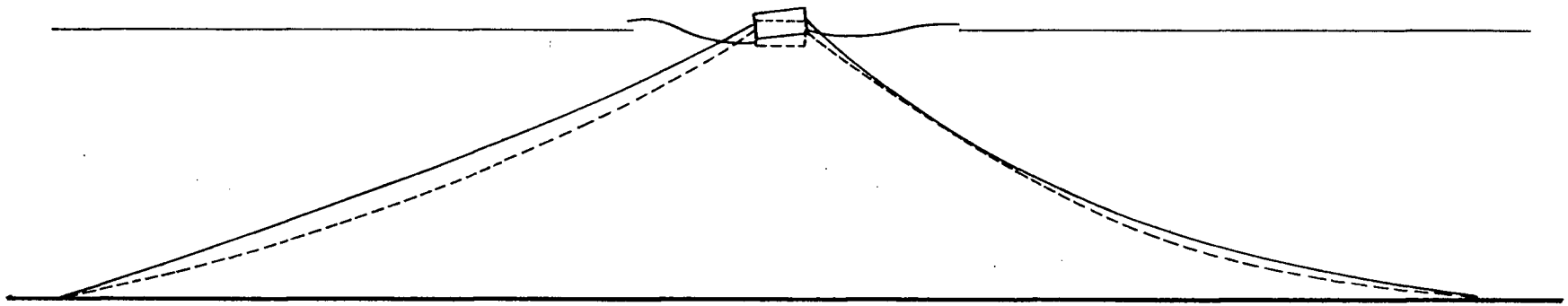

----- equilibrium position with drift force

——— instantaneous position

$B/\lambda = 0.35$

$h_i/\lambda = 0.1$

$C/d = 2.83$

$\omega t = 70^0$

$K_t = 0.24$

TYPICAL COMPUTER PLOT

FIGURE 8

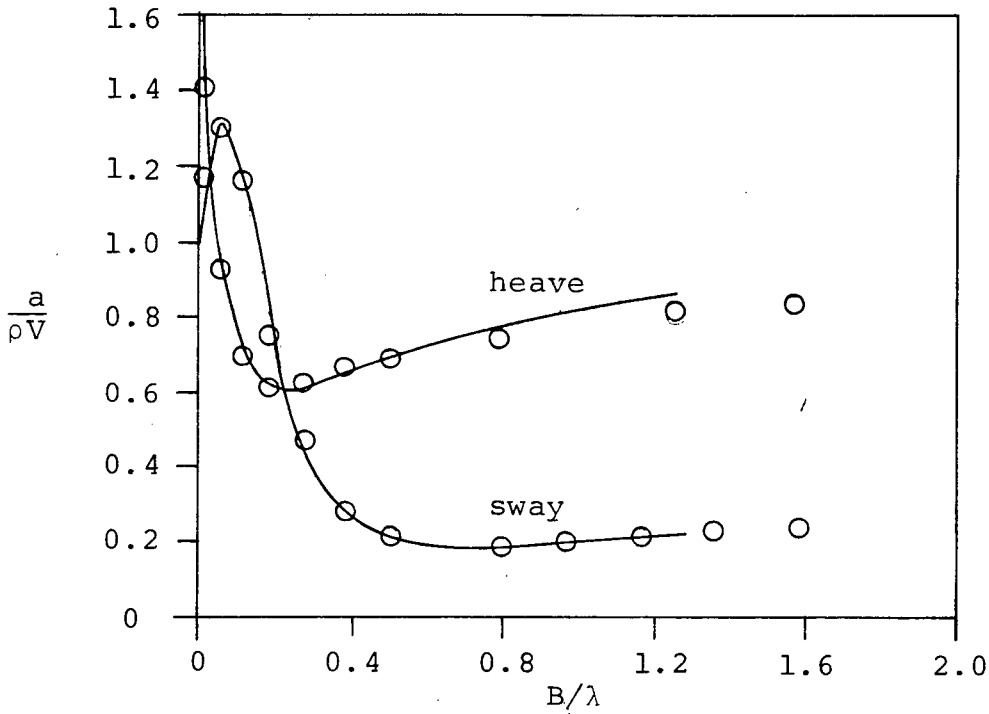

ADDED MASS

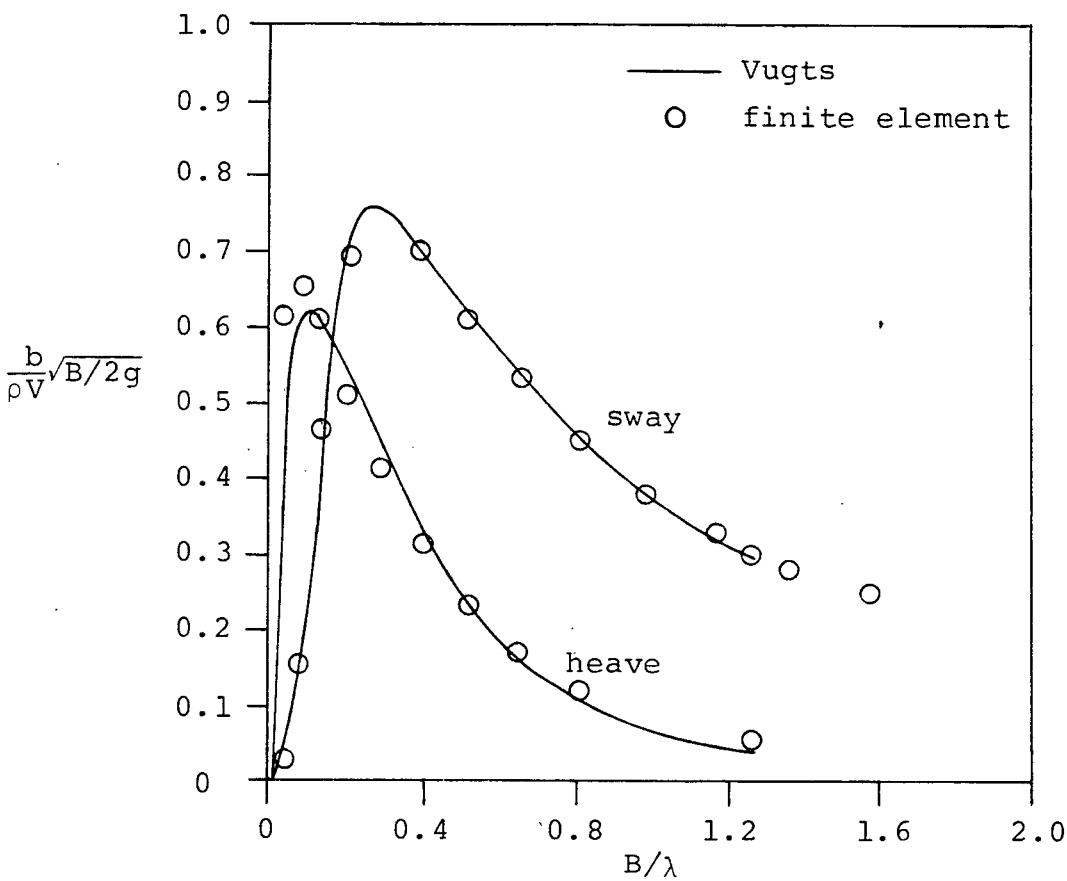

DAMPING

ADDED MASS AND DAMPING - CIRCULAR CYLINDER

FIGURE 9

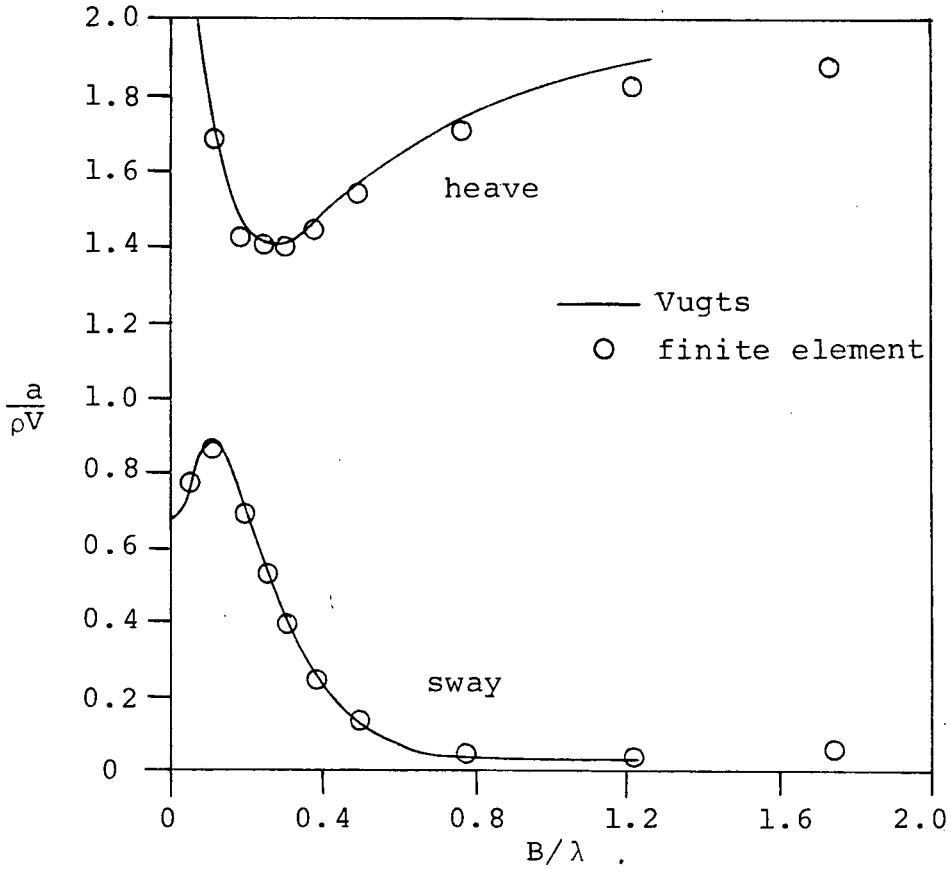

ADDED MASS

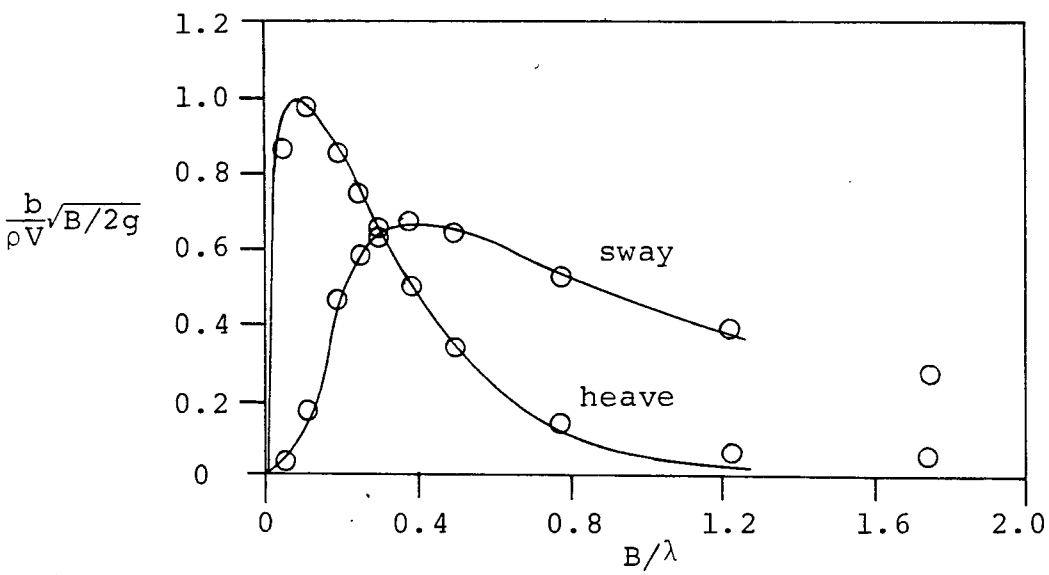

DAMPING

ADDED MASS AND DAMPING - RECTANGULAR CYLINDER (B/D = 4.0)

FIGURE 10

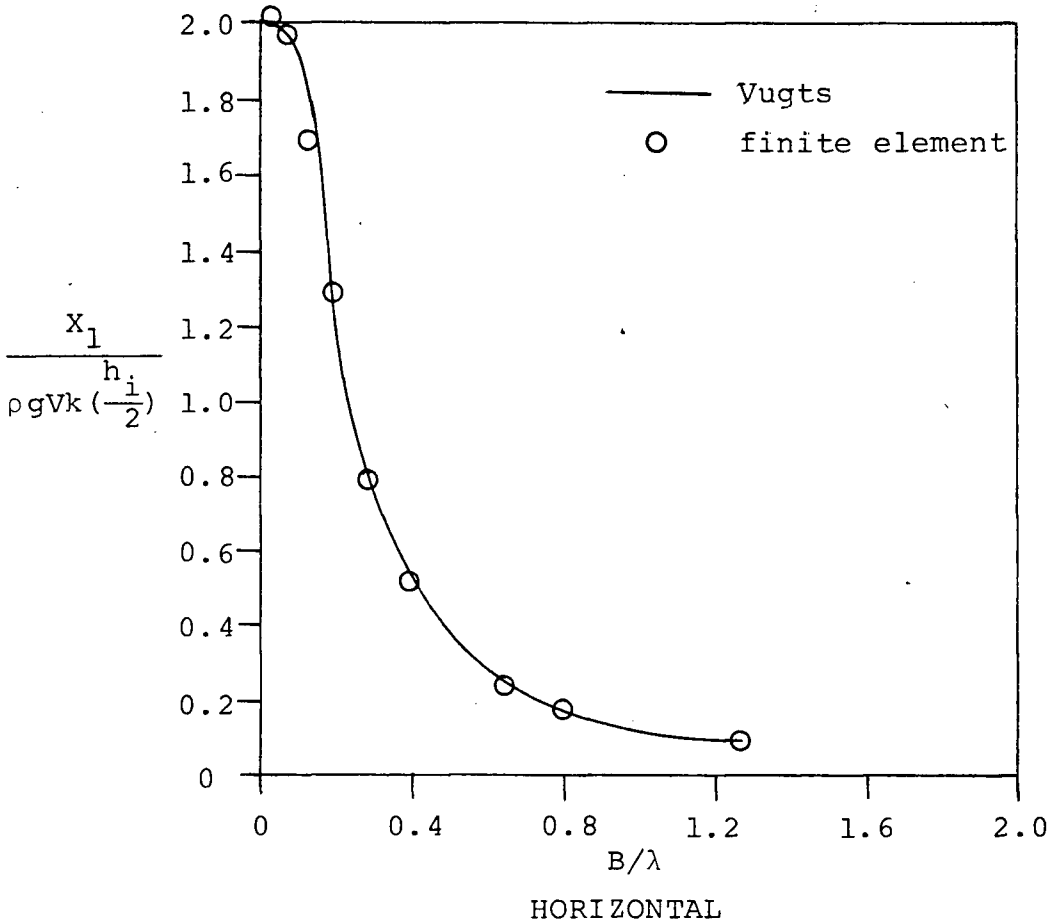

HORIZONTAL

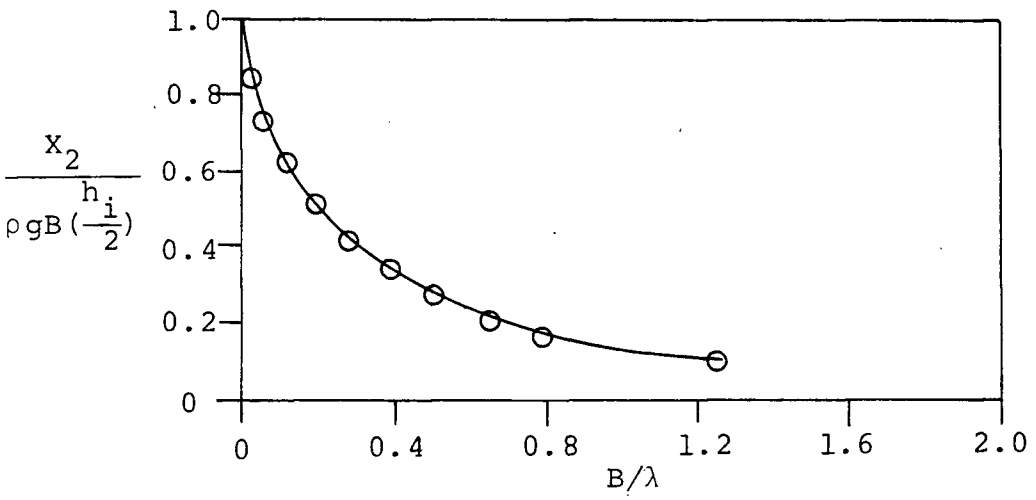

VERTICAL

EXCITING FORCES - CIRCULAR CYLINDER

FIGURE 11

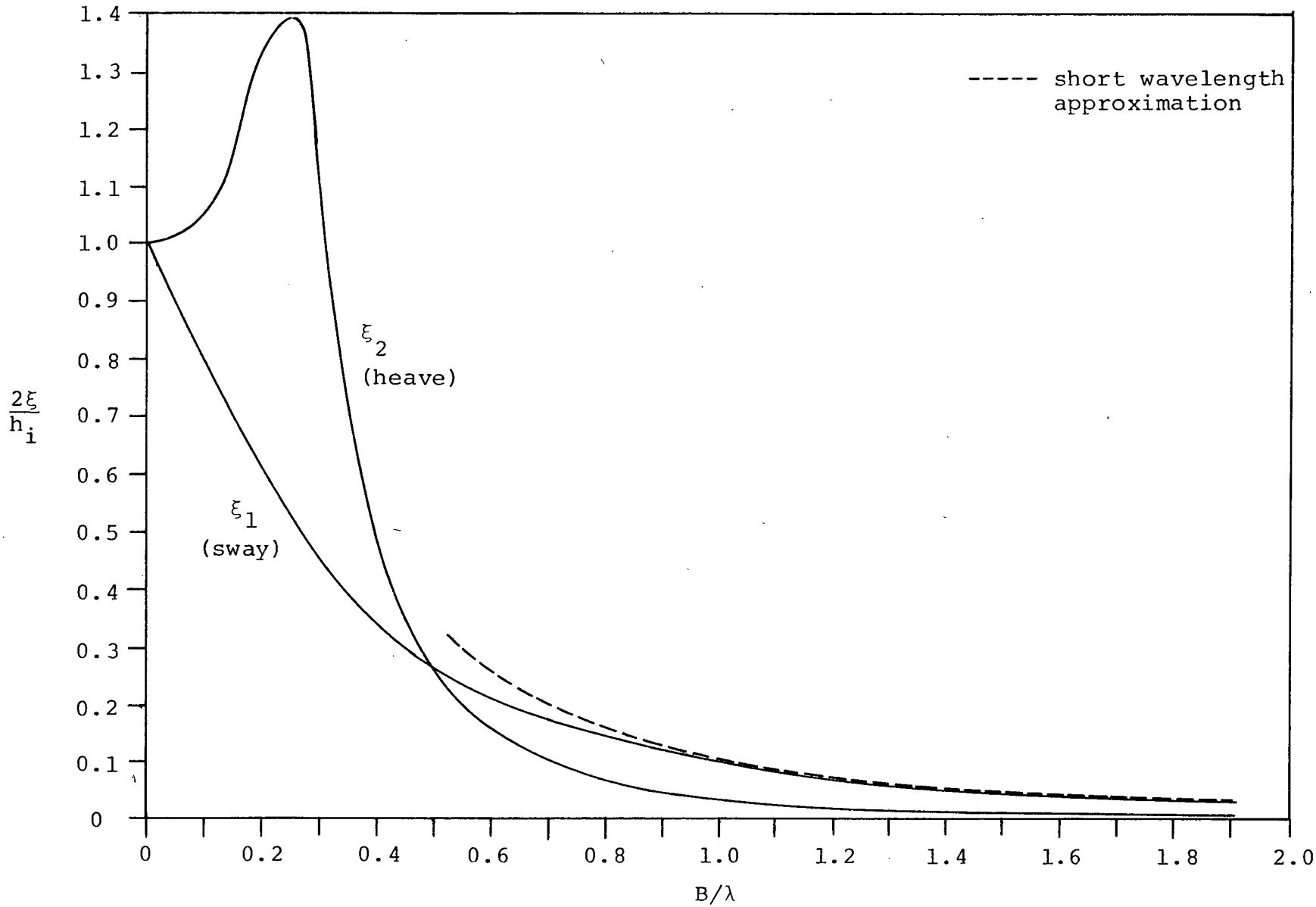

AMPLITUDES OF MOTION - CIRCULAR CYLINDER

FIGURE 12

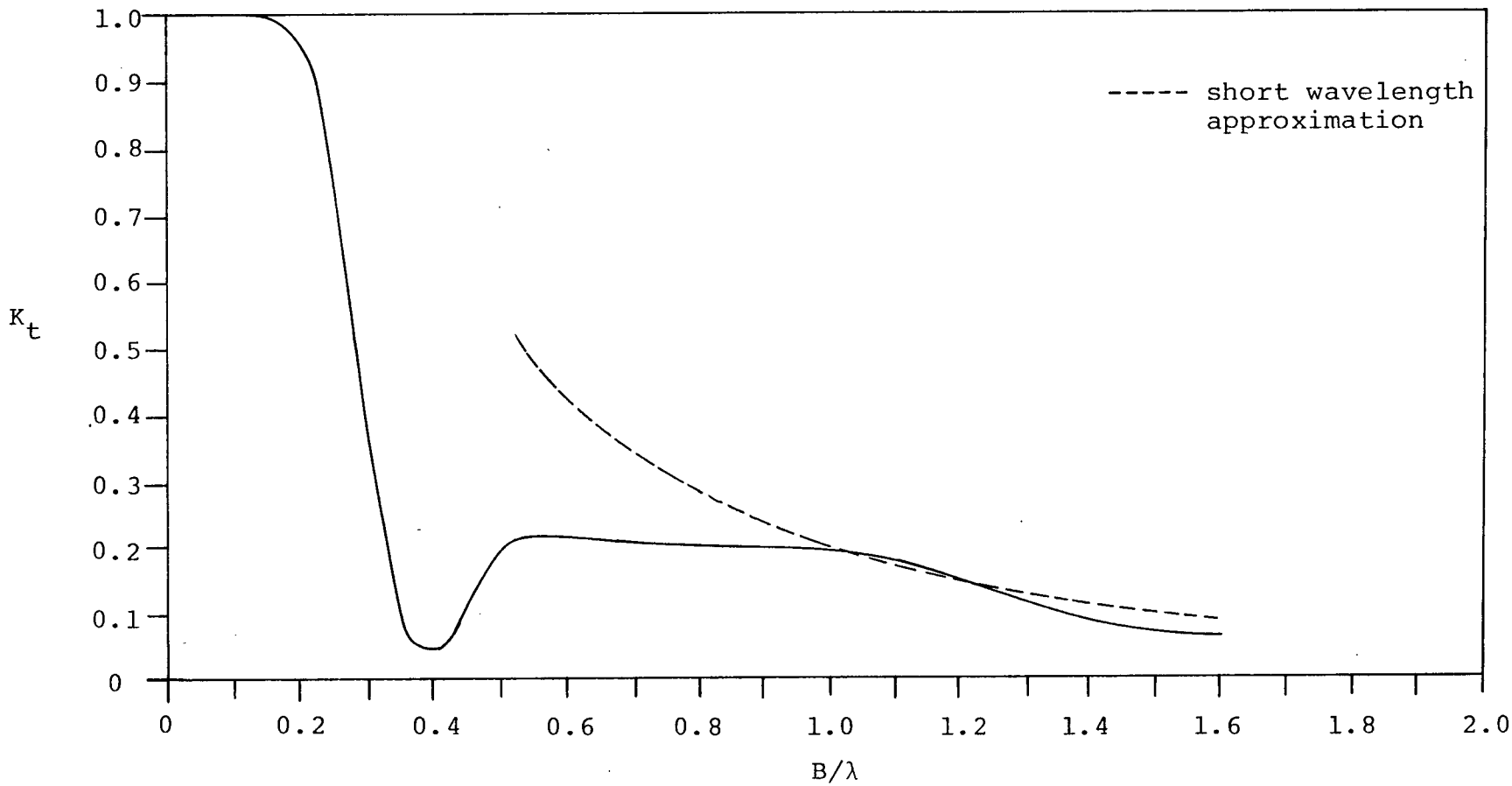

TRANSMISSION COEFFICIENT - CIRCULAR CYLINDER

FIGURE 13

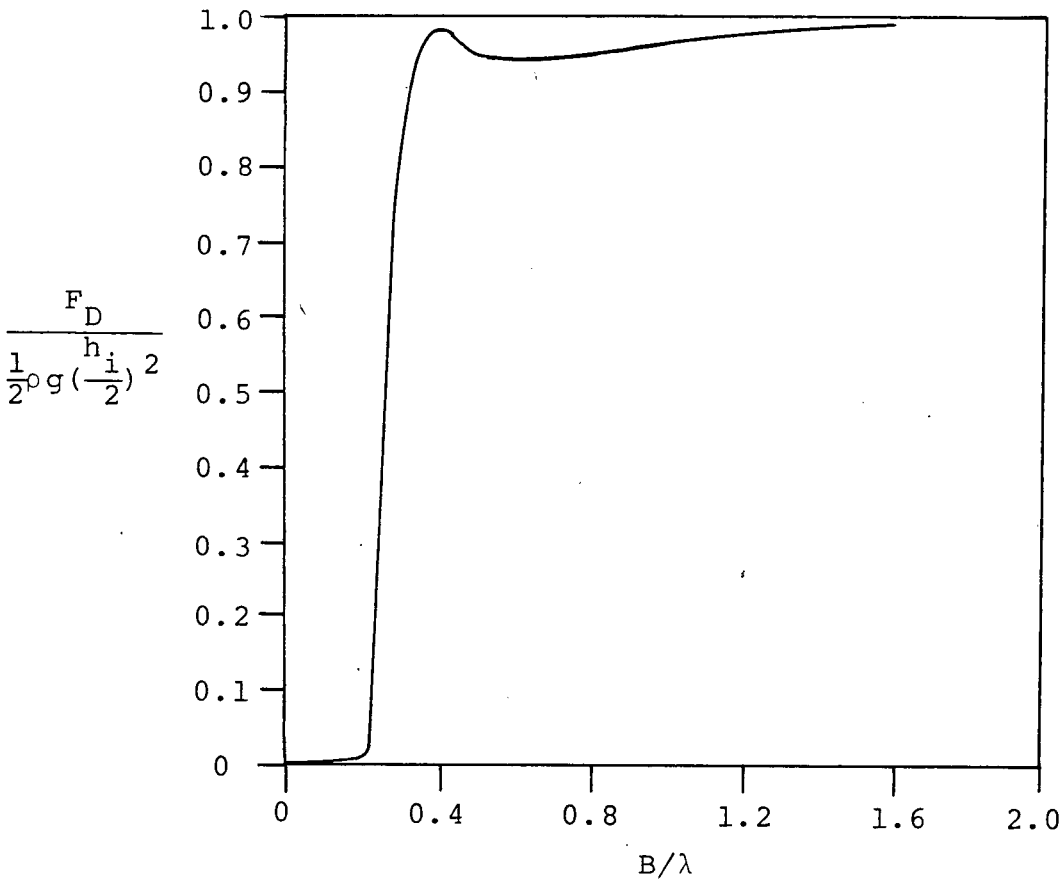

DRIFT FORCE - CIRCULAR CYLINDER

FIGURE 14

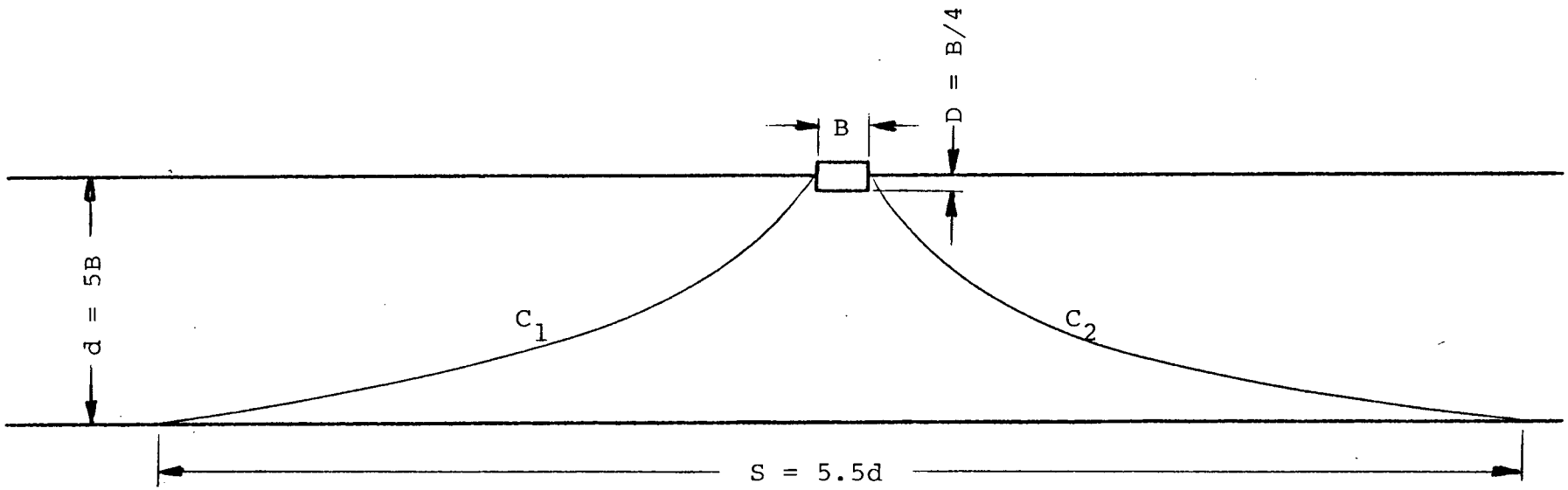

GENERAL ARRANGEMENT - RECTANGULAR BREAKWATER

FIGURE 15

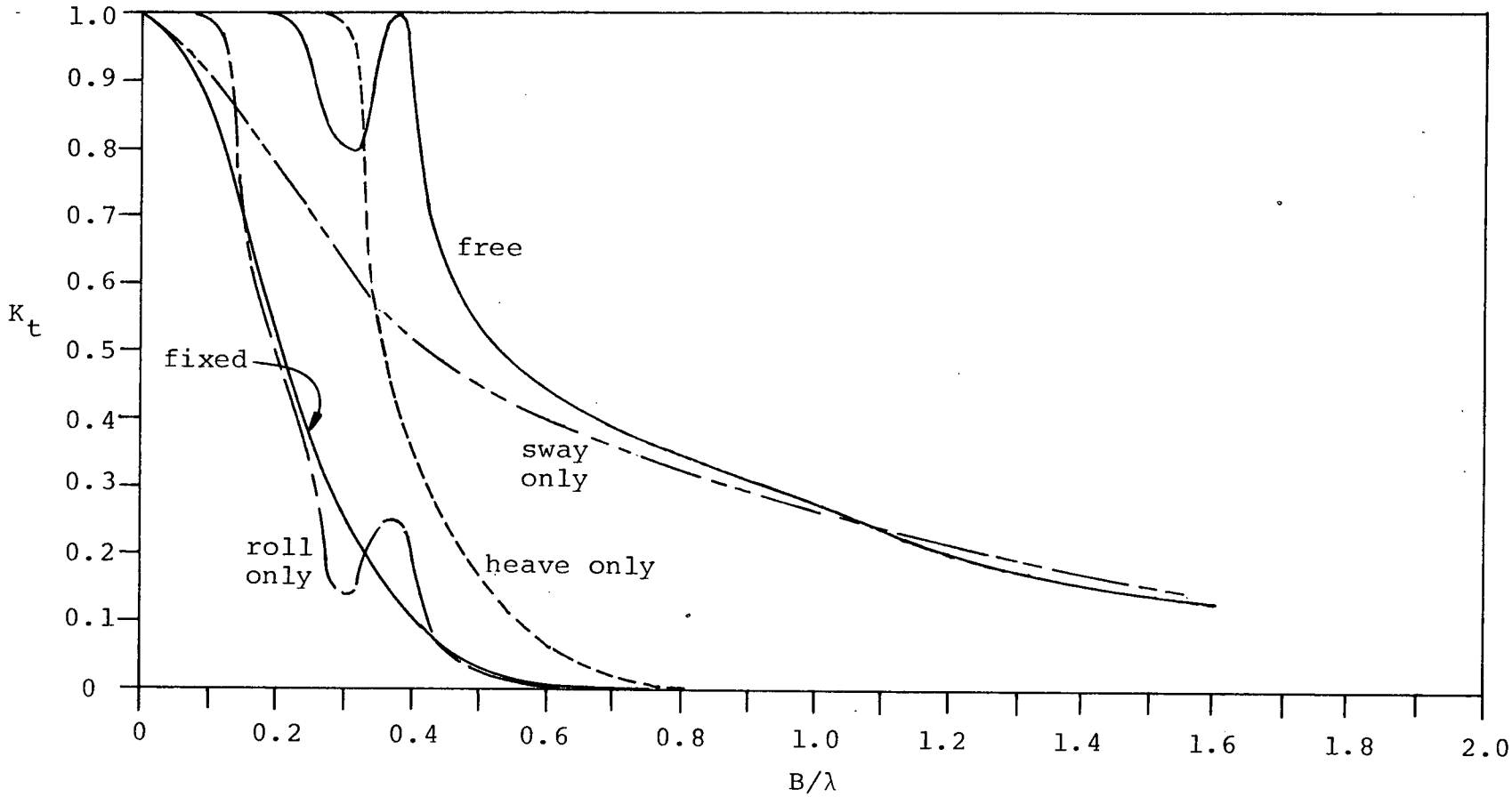

CONTRIBUTION OF MODES TO TRANSMITTED WAVE

FIGURE 16

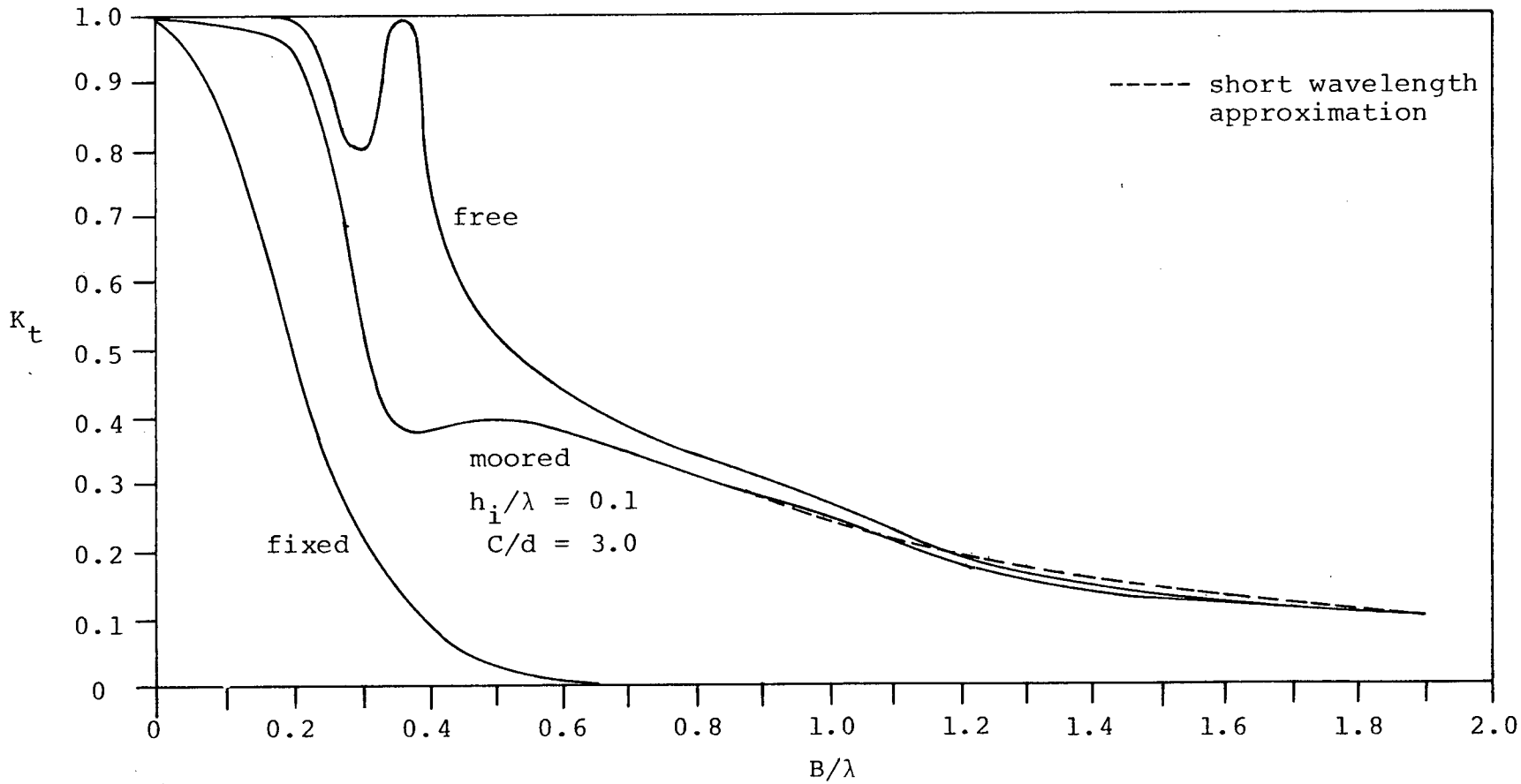

SLACK-MOORED TRANSMISSION COEFFICIENT

FIGURE 17

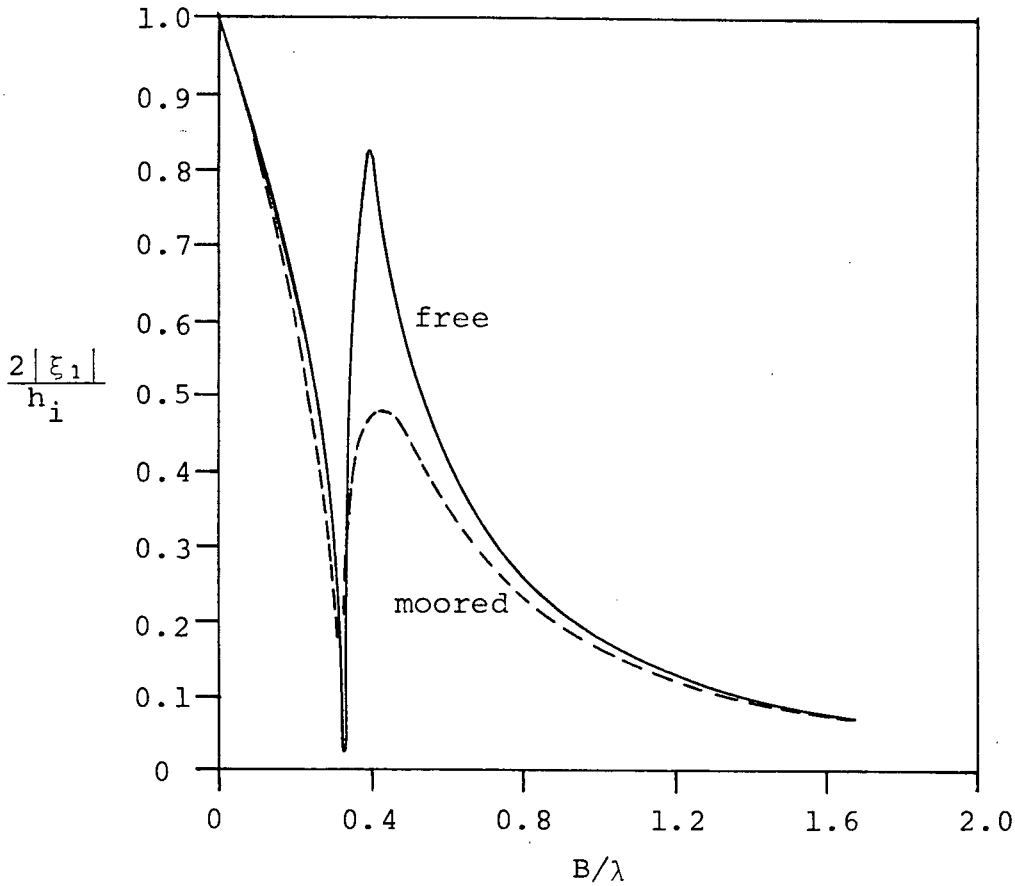

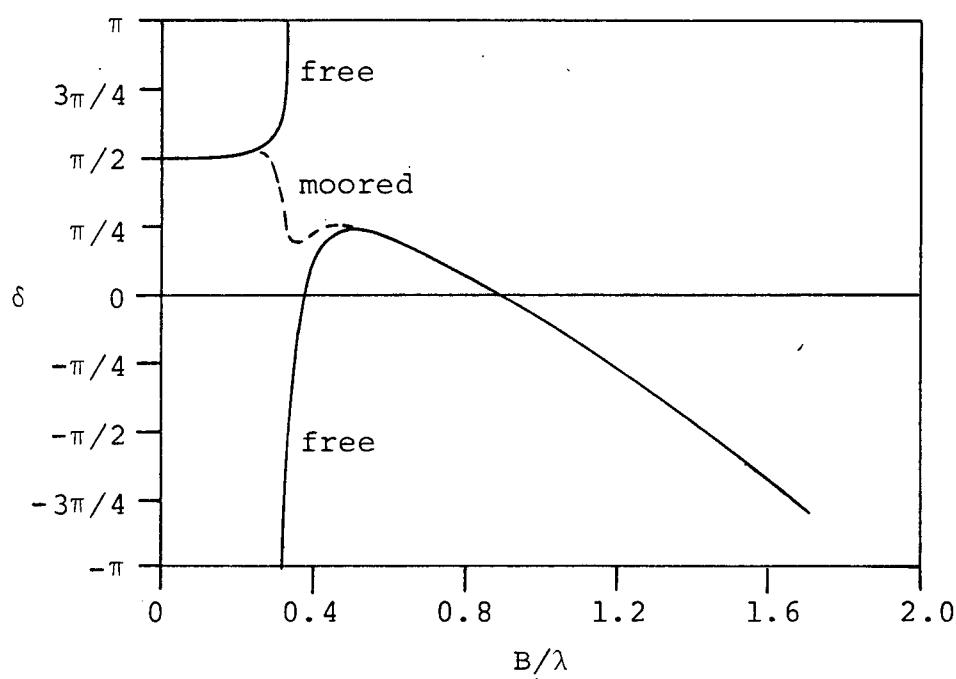

SWAY AMPLITUDE AND PHASE ANGLE

FIGURE 18

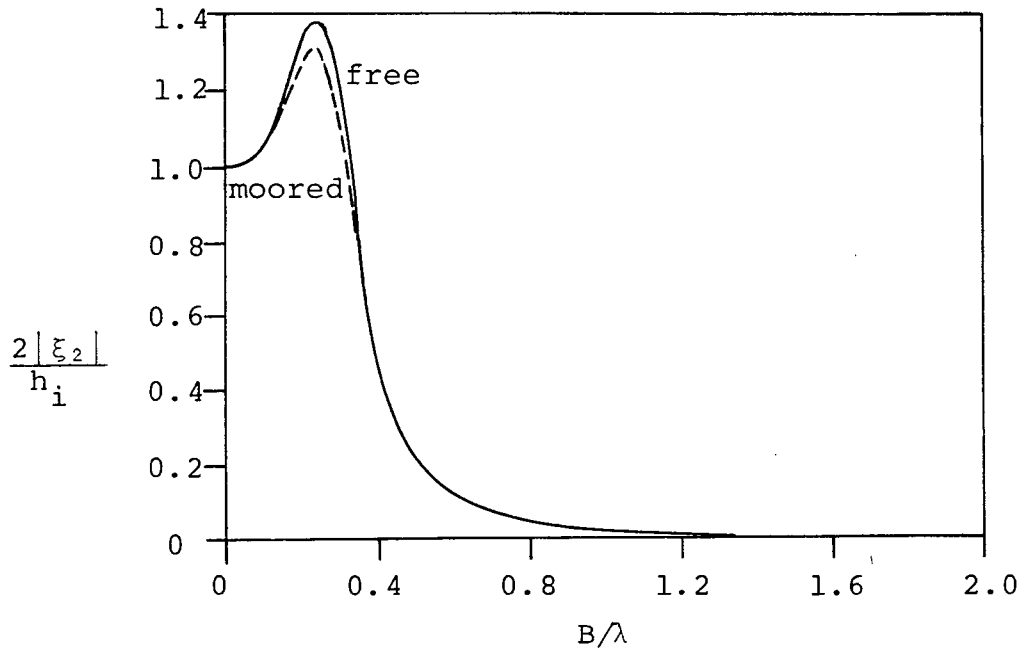

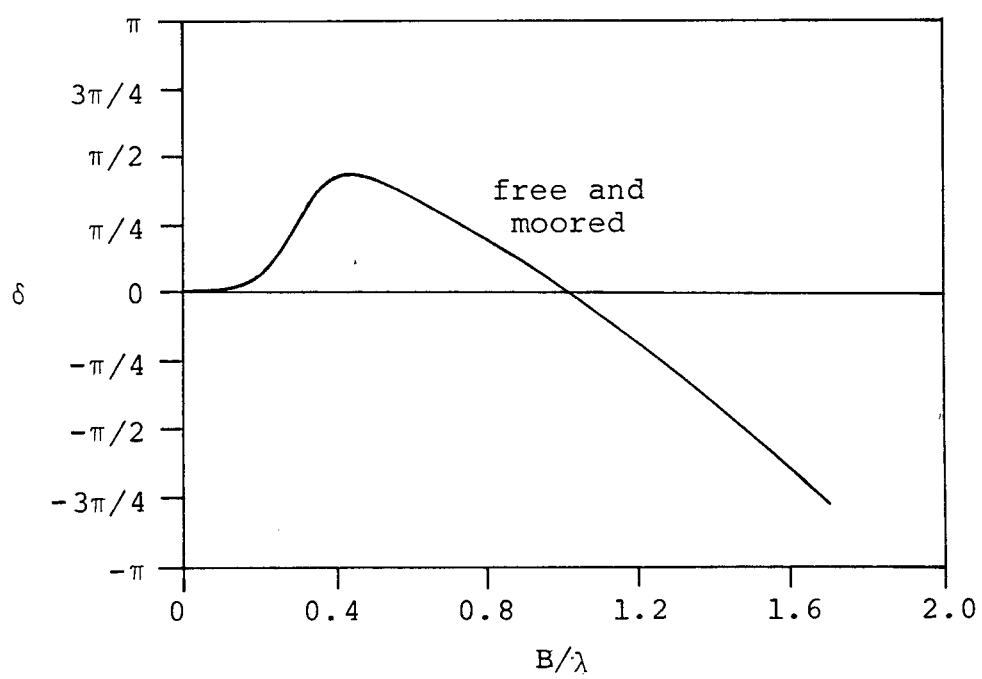

HEAVE AMPLITUDE AND PHASE ANGLE

FIGURE 19

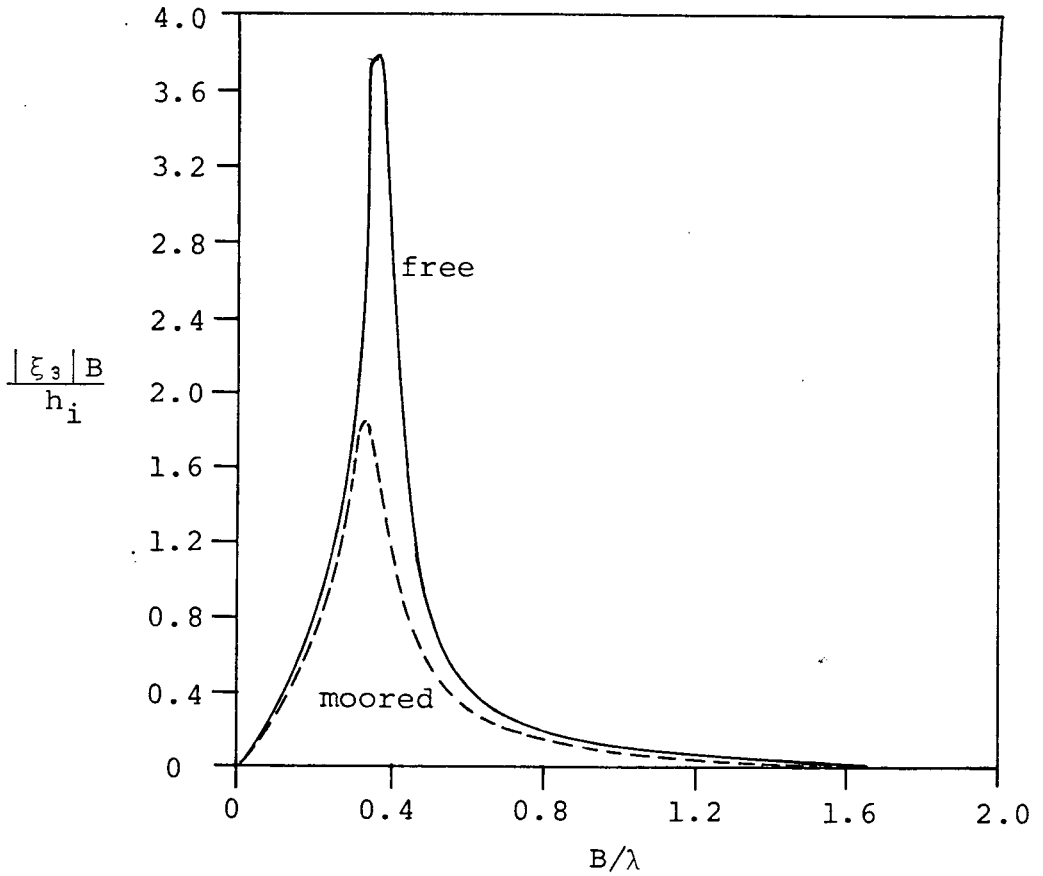

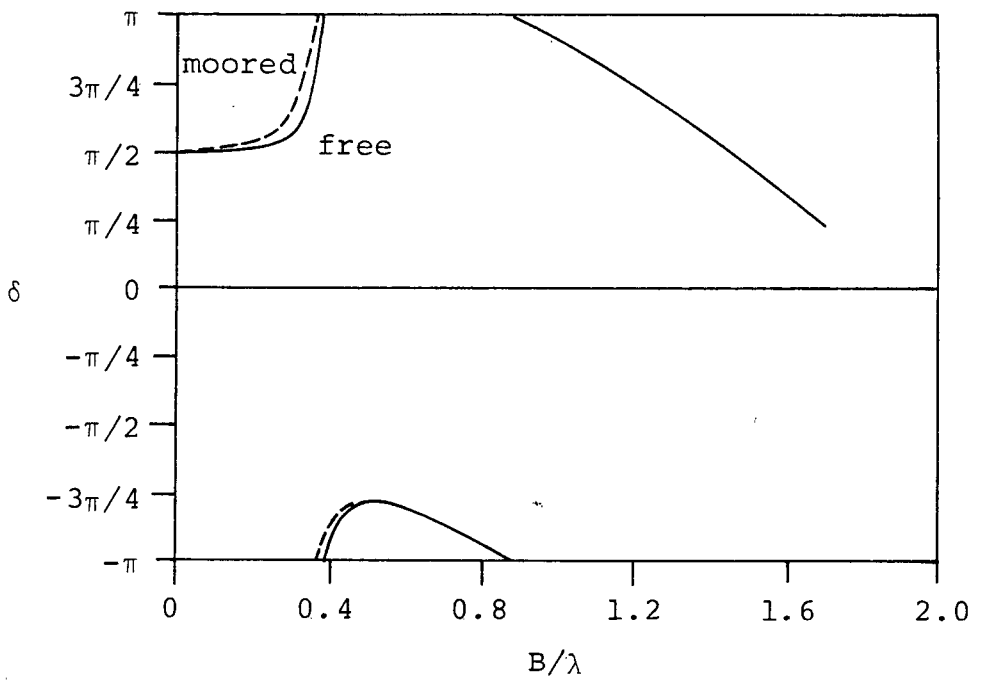

ROLL AMPLITUDE AND PHASE ANGLE

FIGURE 20

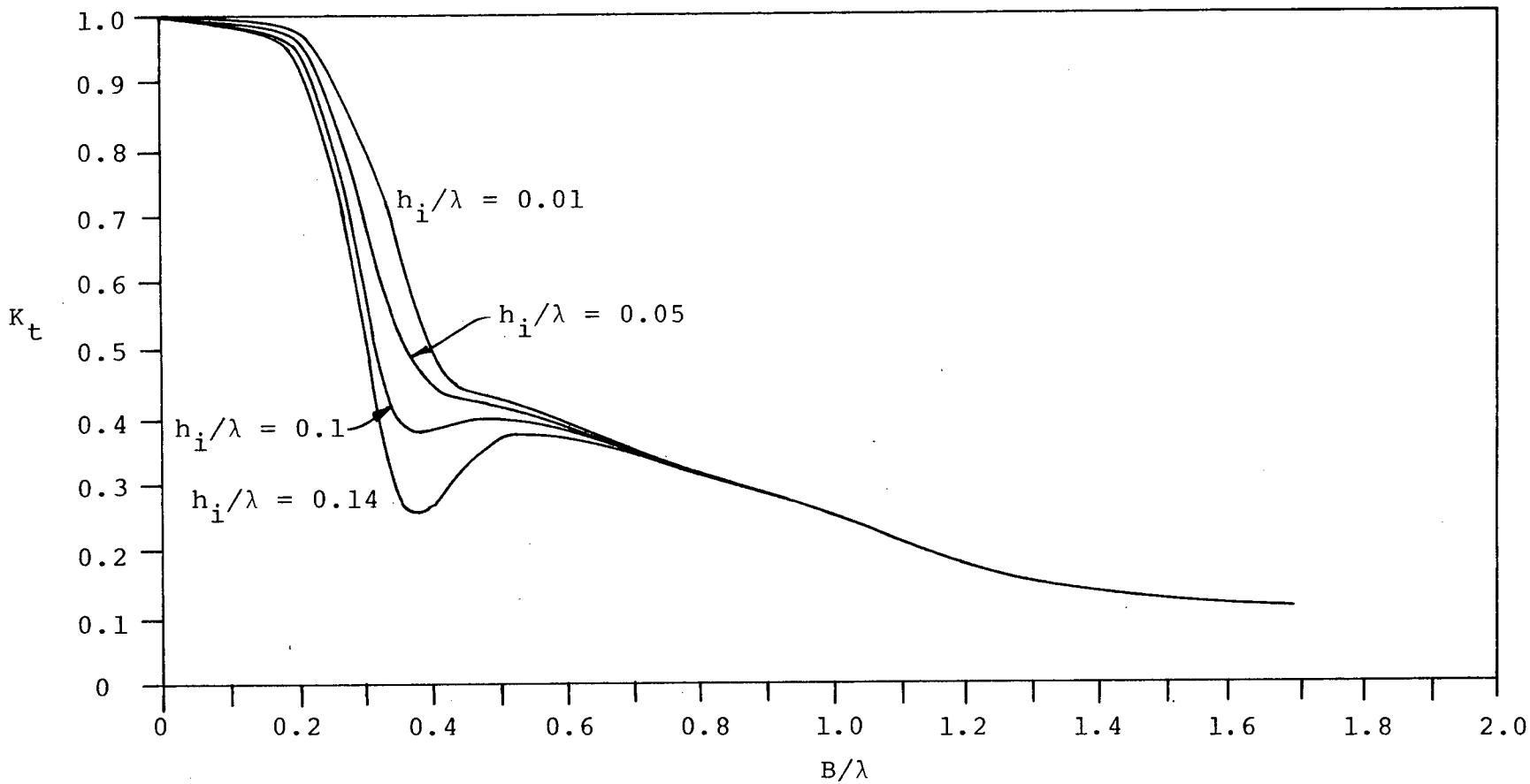

EFFECT OF WAVE STEEPNESS

FIGURE 21

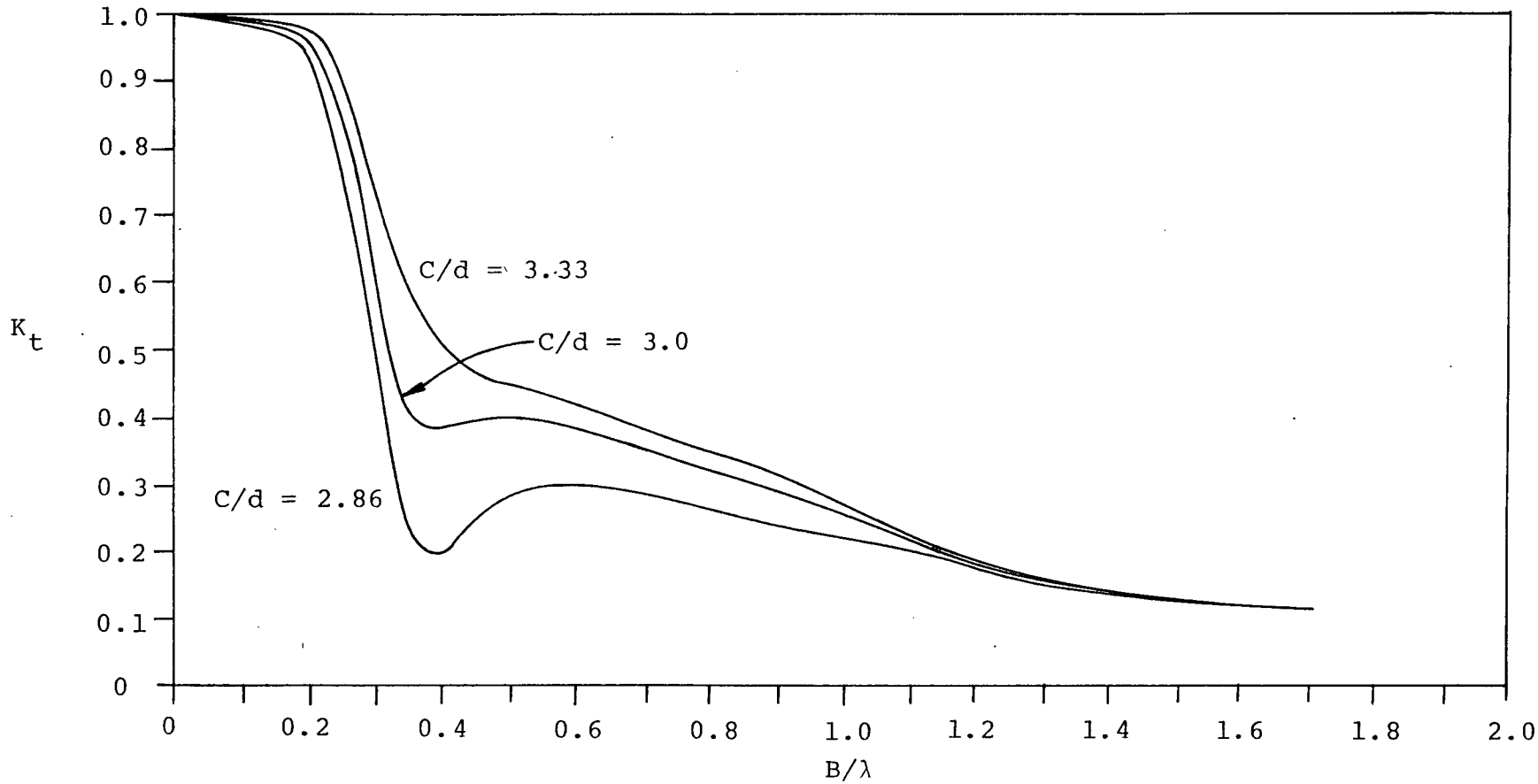

EFFECT OF CABLE TAUTNESS

FIGURE 22

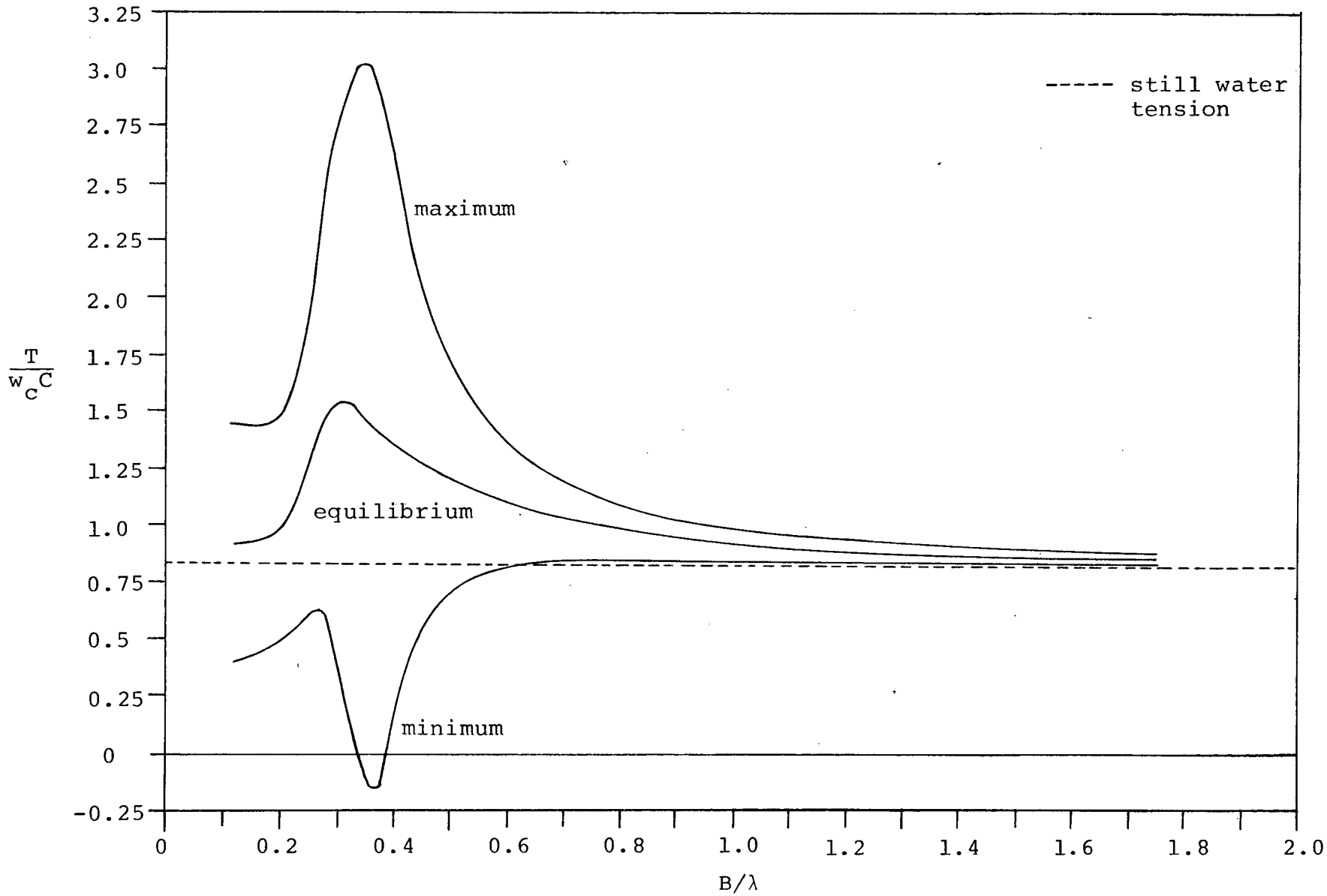

SEAWARD CABLE TENSION
FIGURE 23

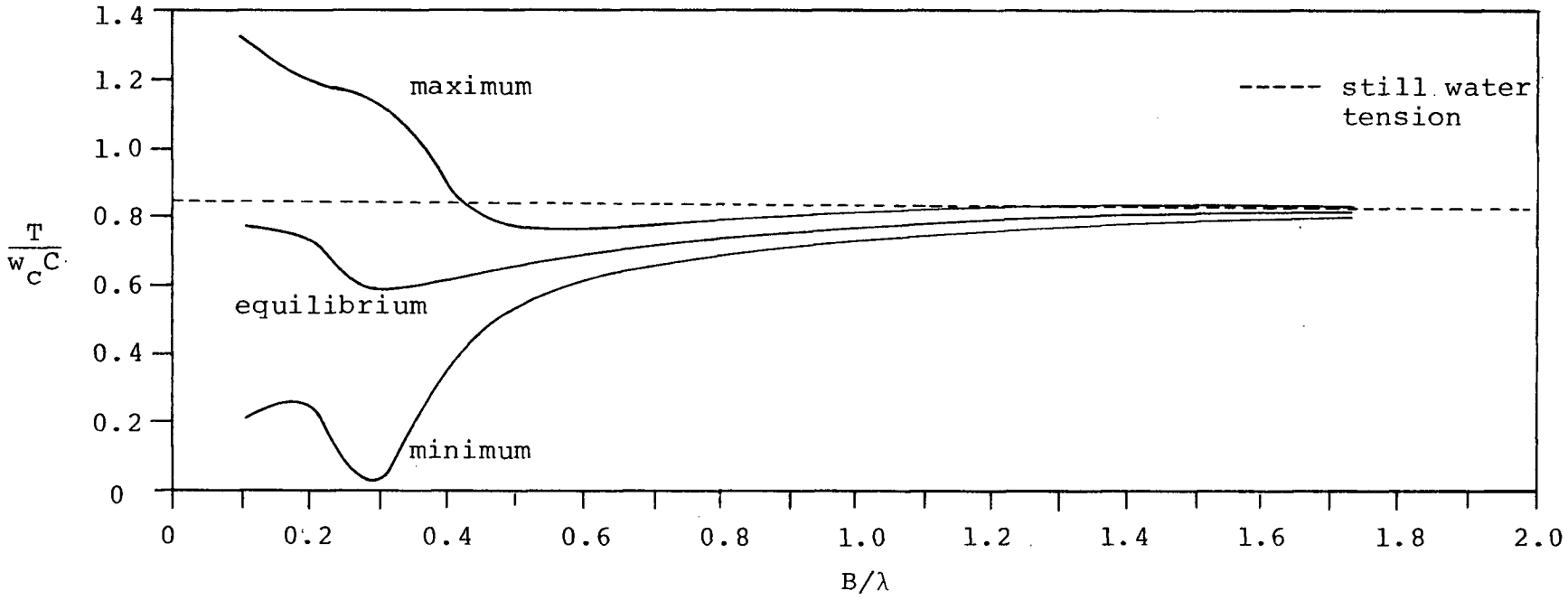

SHOREWARD CABLE TENSION

FIGURE 24

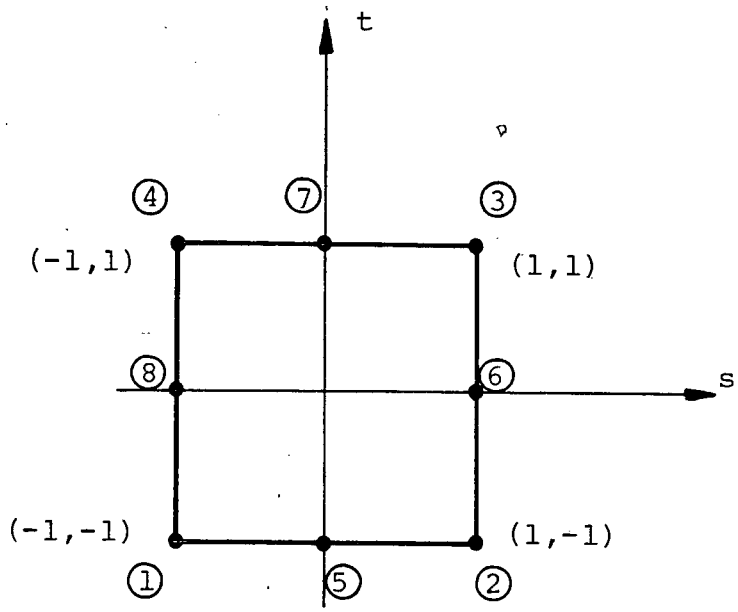

TRANSFORMED COORDINATE SYSTEM

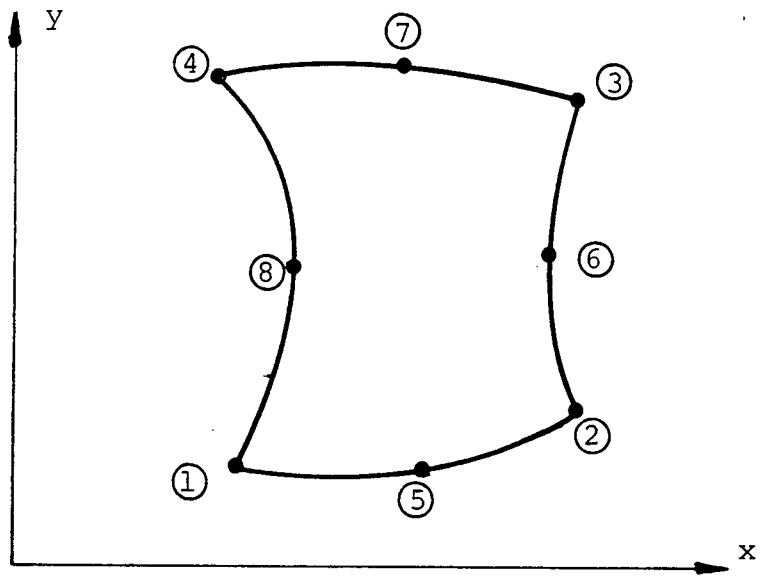

GLOBAL COORDINATE SYSTEM

QUADRATIC ISOPARAMETRIC ELEMENT

FIGURE A-1

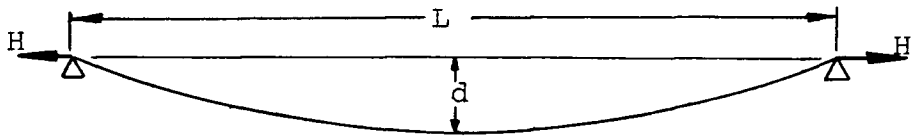

$$\frac{L}{\frac{HL_e}{(AE)}} = \begin{matrix} 0.13\text{x}10^6 \text{ (inextensible)} \\ 0.13\text{x}10^2 \text{ (extensible)} \end{matrix} \qquad \frac{L}{d} = 10$$

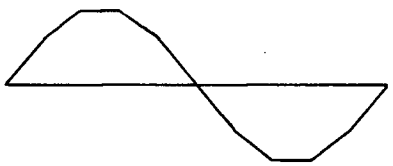

$\beta L = 6.07$
(6.29)

$\beta L = 4.01$
(4.07)

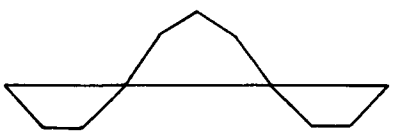

$\beta L = 9.18$
(8.98)

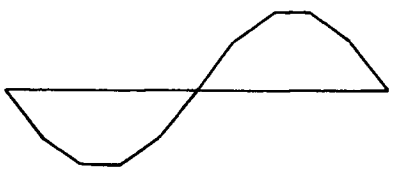

$\beta L = 6.01$
(6.29)

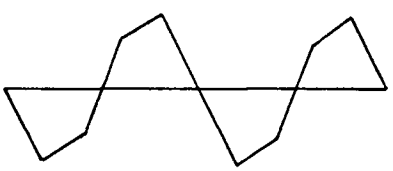

$\beta L = 13.08$
(12.57)

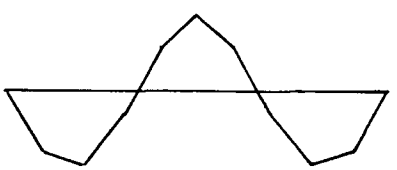

$\beta L = 9.56$
(9.46)

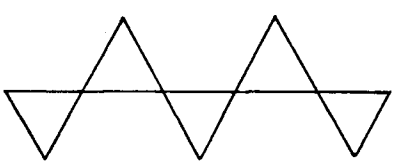

$\beta L = 16.79$
(15.44)

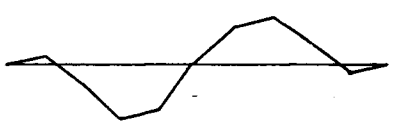

$\beta L = 11.80$
(12.57)

INEXTENSIBLE

EXTENSIBLE

NATURAL FREQUENCIES AND MODE SHAPES

FIGURE B-1